ELEMENTA Science of the Anthropocene

McLaughlin, K, et al. 2021. Influence of anthropogenic nutrient inputs on rates of coastal ocean nitrogen and carbon cycling in the Southern California Bight, United States. *Elem Sci Anth*, 9: 1. DOI: https://doi.org/10.1525/elementa.2020.00145

RESEARCH ARTICLE

Influence of anthropogenic nutrient inputs on rates of coastal ocean nitrogen and carbon cycling in the Southern California Bight, United States

Karen McLaughlin[1,*], Meredith D. A. Howard[1,2], George Robertson[3], Carly D. A. Beck[1,4], Minna Ho[1], Fayçal Kessouri[1], Nikolay P. Nezlin[1,5], Martha Sutula[1], and Stephen B. Weisberg[1]

Coastal nitrogen enrichment is a global environmental problem that can influence acidification, deoxygenation, and subsequent habitat loss in ways that can be synergistic with global climate change impacts. In the Southern California Bight, an eastern boundary upwelling system, modeling of wastewater discharged through ocean outfalls has shown that it effectively doubles nitrogen loading to urban coastal waters. However, effects of wastewater outfalls on rates of primary production and respiration, key processes through which coastal acidification and deoxygenation are manifested, have not been directly linked to observed trends in ambient chlorophyll *a*, oxygen, or pH. Here, we follow a "reference-area" approach and compare nutrient concentrations and rates of nitrification, primary production, and respiration observed in areas within treated wastewater effluent plumes to areas spatially distant from ocean outfalls where we expected minimal plume influence. We document that wastewater nutrient inputs had an immediate, local effect on nutrient stoichiometry, elevating ammonium and nitrite concentrations by 4 μM and 0.2 μM (on average), respectively, and increasing dissolved nitrogen-to-phosphorus ratios 7-fold within the plume. Chlorophyll *a* increased slightly by 1 μg L^{-1} in the upper 60 m of the water column (on average), and $\delta^{13}C$ and δ^{15} N of suspended particulate matter, an integrated measure of primary production, increased by 1.3% and 1%, respectively (on average). Nitrification rates within the plume increased by 17 nmol L^{-1} day^{-1} (on average). We did not observe a significant near-plume effect on $\delta^{18}O$ and δ^{15} N of dissolved nitrate + nitrite, an indicator of nitrogen assimilation into biomass, on rates of primary production and respiration or on dissolved oxygen concentration, suggesting that any potential impact from wastewater on these key features is moderated by other factors, notably water mass mixing. These results indicate that a "reference-area" approach may be insufficient to document regional-scale impacts of nutrients.

Keywords: Wastewater, Eutrophication, Biogeochemistry, Nutrient cycles, Coastal ocean

Introduction

Globally, offshore ocean outfalls have been considered an effective and reliable strategy for disposing of treated industrial and domestic wastewater (Wood et al., 1993; Roberts et al., 2010). However, wastewater effluent released through these outfalls is rarely treated to remove nutrients and, consequently, ocean outfalls have been implicated in eutrophication of coastal waters (Roberts et al., 2010; Powley et al., 2016; Valiela et al., 2016). Eutrophication can have impacts on coastal habitats that are synergistic with global changes, such as increasing frequency and occurrence of algal blooms (Howarth et al., 2002; Glibert et al., 2006), coastal acidification (Borges and Gypens, 2010; Wallace et al., 2014), and deoxygenation (Rabalais et al., 2014; Breitburg et al., 2018) through enhanced heterotrophic respiration rates. Given appropriate light and temperature conditions, eutrophication initially causes a temporary drawdown of CO_2 concentrations at the surface due to the intense biological productivity of the associated algal bloom (Borges and Gypens, 2010). Subsequently, eutrophication lowers pH because it provides conditions for greater heterotrophic respiration rates (i.e., decomposition, also referred to as remineralization) by organisms such as bacteria. This respiration process

[1] Southern California Coastal Water Research Project, Costa Mesa, CA, USA

[2] Present affiliation: Central Valley Regional Water Quality Control Board, Rancho Cordova, CA, USA

[3] Orange County Sanitation District, Fountain Valley, CA, USA

[4] Present affiliation: California Department of Fish and Wildlife, Ontario, CA, USA

[5] Present affiliation: Global Science & Technology, Inc., Greenbelt, MD, USA

* Corresponding author:
Email: karenm@sccwrp.org

oxidizes organic matter, draws down local oxygen levels, releases CO_2, and—in extreme cases—can lead to hypoxic dead zones (Diaz and Rosenberg, 2008). The water-depth of the pH change associated with anthropogenic eutrophication is a function of where organic matter is respired. In many shallow coastal shelf systems, this acidification occurs at or near the bottom sediments, where organic matter is oxidized (Waldbusser et al., 2010; Sunda and Cai, 2012). In the absence of global strategies to mitigate coastal ocean changes, local managers are being urged to consider the management of local, land-based nutrient sources to slow the progression of acidification and deoxygenation and their impact on coastal habitats (Kelly et al., 2011; Strong et al., 2014; Chan et al., 2016).

The role of coastal nutrient discharges and coastal eutrophication in exacerbating coastal acidification and deoxygenation is well documented, including the East China Sea and the Gulf of Mexico (Cai et al., 2011), the Baltic Sea (Sunda and Cai, 2012), the nearshore regions of the North Sea (Provoost et al., 2010), and the Chesapeake Bay (Waldbusser, 2011). However, in an eastern boundary upwelling system, strong upwelling and vigorous surface currents have been thought to limit the impacts of local anthropogenic nutrient inputs (Chavez and Messié, 2009; Capone and Hutchins, 2013; Fennel and Testa, 2019). Recent evidence from the Southern California Bight (SCB) has challenged this thinking for this highly urbanized coastline. In the SCB, on an annual basis, 92% of terrestrial N flux is wastewater effluent from publicly owned treatment works, most of which is discharged directly into coastal waters via a relatively small number of outfall pipes (Sutula et al., 2021). Modeled outfall N loads are roughly equivalent to those from upwelling in urbanized sections of the coast, effectively doubling N loading to the shelf (Howard et al., 2014). These inputs have an immediate, local effect on nitrification rates as high concentrations of wastewater ammonium are rapidly nitrified in the subsurface plumes (McLaughlin et al., 2017). More broadly, observational evidence has shown an increase in the extent of algal blooms in the SCB over the last decade, with chronic blooms documented in areas colocated with major inputs of anthropogenic nutrients (Schnetzer et al., 2007; Nezlin et al., 2012; Schnetzer et al., 2013). Analysis of a decade of quarterly ocean surveys across the central and northern SCB has shown a significant decrease in dissolved oxygen (DO) concentrations (Bograd et al., 2008), and the rate of decline in the nearshore, proximal to treated wastewater effluent outfalls, has been faster than offshore regions (Booth et al., 2014). However, these regional-scale observations can also be influenced by climate change and Pacific Basin-scale drivers (Booth et al., 2014; Nezlin et al., 2018), and neither ambient chlorophyll *a*, DO, or pH have been linked specifically to an effect of wastewater outfalls on rates of primary production and respiration—key processes through which coastal acidification and deoxygenation are manifested.

In this article, we quantified nutrient forms, concentrations, and rates of carbon and nitrogen cycling that ultimately influence eutrophication and coastal acidification and deoxygenation, both within wastewater plumes and in areas spatially distant from plumes. We also explored the environmental factors that may be influencing rates, including seasonal and interannual variability linked to the influence of upwelling. Finally, we employed stable isotope tracers to further track relationships and patterns in N and C cycling in these coastal zones as more integrative measurements to compare to the instantaneous rate measurements. We focused on the effect of wastewater N because the SCB is largely N-limited (Thomas et al., 1974; Cullen and Eppley, 1981) and wastewater point-source discharges dominate anthropogenic sources (Howard et al., 2014) and contain high concentrations of nitrogenous species. As a core part of our study design, observations of ambient ocean state and rates were made in two types of regions defined by the probability of plume impact: (1) "nearfield" regions, defined as the region of active effluent plume mixing and dispersion within 10 km of the outfall and (2) "farfield" regions, defined as the region where ambient ocean flow and biogeochemical conditions dominate and the effluent plume is expected to exert minimal influence on carbon and nitrogen cycling.

The value of such observations extends beyond the testing of the hypothesis that wastewater plumes affect water column biogeochemical parameters (pH, DO, chlorophyll *a*) and rates of nutrient and carbon cycling. To support California's climate action strategies, a spatially explicit, 3-dimensional numerical ocean model of the SCB was developed and is being applied to examine the relative effects of climate change, natural climate cycles, and local terrestrial and atmospheric carbon and nutrient inputs (Kessouri et al., 2020; Deutsch et al., 2021). However, in order to support conversations on the utility of nutrient management as a climate change mitigation strategy, such models must be validated carefully against observations of biogeochemical state and rate data. Inadequate numerical model validation has been identified as a significant barrier to effective, evidence-based solutions to coastal eutrophication (Boesch, 2019). Models must not only reproduce observed state data successfully, they must also reproduce observed biogeochemical rate data successfully, ensuring that the model is predicting the appropriate state variables for the right reasons. Thus, these observations are part of a coupled observational-numerical modeling approach characterizing the effect of local nutrient and carbon inputs on SCB coastal habitats, laying the foundation for evidence-based solutions for coastal acidification and deoxygenation.

Materials and methods

Study region

The SCB is the bend in the coastline between Point Conception (34.45°N) and the U.S.–Mexico International Border (32.44°N). It is situated in the California Current System on the U.S. Pacific Coast. As an eastern boundary upwelling system, the SCB is a biologically productive region of high economic and ecological importance. Seasonal spring upwelling of nutrient-rich deep water maintains high rates of biological productivity over broad scales. At the same time, upwelling draws water masses that are low in DO, pH, and carbonate saturation state

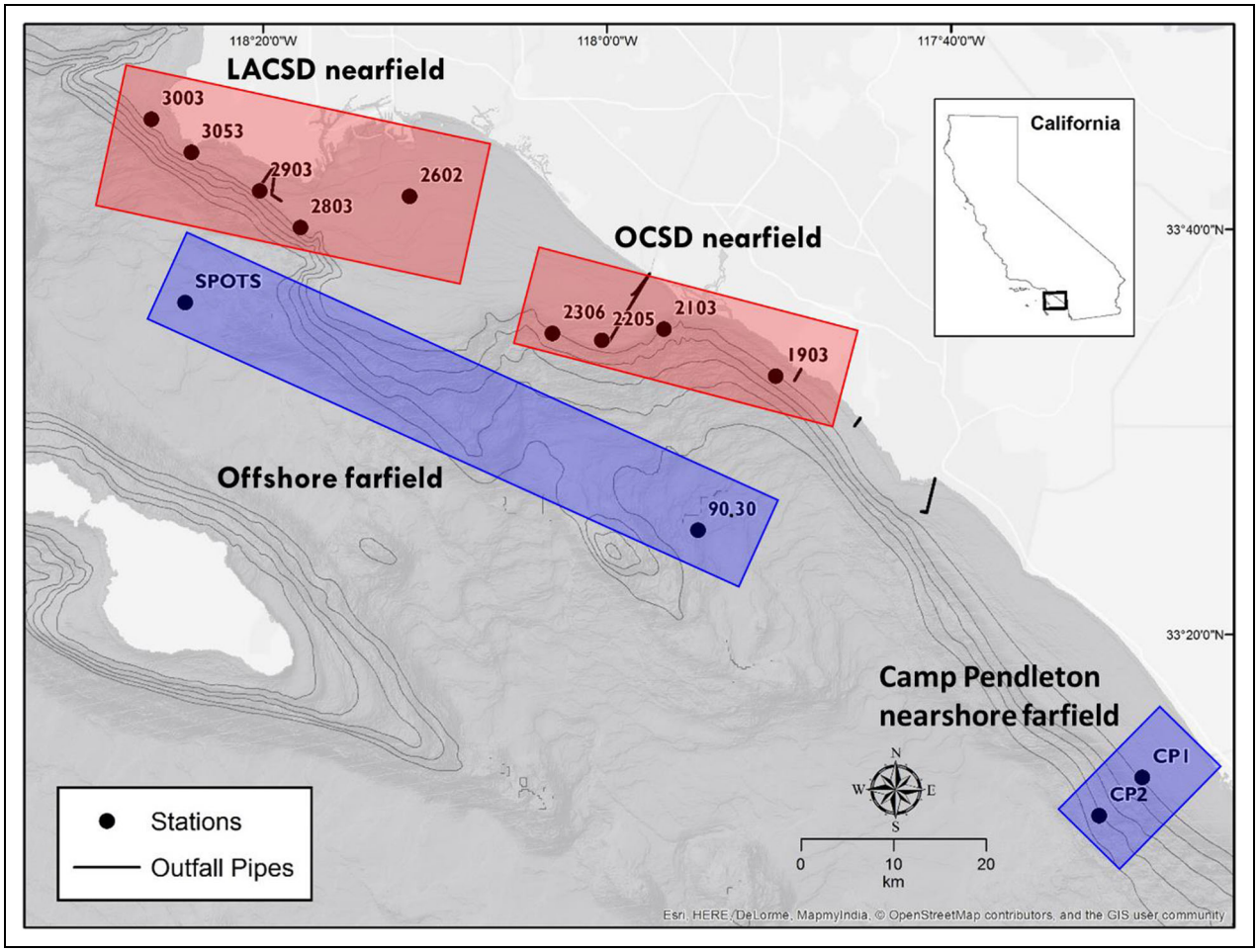

Figure 1. Station locations. The nearfield subregions are shown in red and include grid stations for the Los Angeles County Sanitation Districts (LACSD) and Orange County Sanitation District (OCSD). The farfield (reference) subregions spatially distant from the outfalls (short black lines) are shown in blue and include two offshore stations (San Pedro Ocean Time Series and California Cooperative Oceanic Fisheries Investigations 90.30) and two nearshore stations located by Camp Pendleton, in northern San Diego County (CP1 and CP2). Conductivity-temperature-depth casts were collected at additional stations within the regulatory monitoring grids around both the LACSD and OCSD ocean outfalls to determine the location of the plume at the time of sampling to select the second plume station. DOI: https://doi.org/10.1525/elementa.2020.00145.f1

(Ω_{Ar}) onto the shelf and into the photic zone (Sutton et al., 2017). Southern California has a Mediterranean climate with surface runoff confined mostly to the winter, rainy season. The SCB is home to one of the most densely populated coastal regions in North America, where the discharges of treated (advanced primary or secondary) wastewater from a population of over 20 million people are released to the coastal zone via ocean outfalls, along with the urban and agricultural runoff from 72 rivers (Sutula et al., 2021). Modeling efforts have shown that these nutrient sources rival natural upwelling in magnitude (Howard et al., 2014), roughly doubling available N to nearshore coastal waters on an annual basis.

Study design

The study was designed to characterize effects of wastewater plumes on state and rate variables in regions nearfield (within-plume) and farfield (spatially distant) from ocean outfalls where treated wastewater effluent is discharged to the highly urbanized, central portion of the SCB (**Figure 1**). We hypothesized that chemical and biological rates and water chemistry would differ between areas near ocean outfalls (nearfield), where treated wastewater plume was detected, compared to farfield "reference" areas, where the plume could not be detected. Selection of nearfield and farfield locations was informed by previous studies that used colored dissolved organic matter (CDOM) as a tracer of effluent plume (Rogowski et al., 2013; Nezlin et al., 2020); nearfield stations were generally within 10 km of the outfalls, while farfield stations were greater than 10 km away.

We compared water column nutrient profiles and stable isotopic compositions, rates of nitrification, primary production and respiration in nearfield and farfield regions, as well as relationships between parameters and rates and seasonal and interannual differences thereof. Four subregions were sampled, including two nearfield subregions near the Orange County Sanitation District

Table 1. Site information. DOI: https://doi.org/10.1525/elementa.2020.00145.t1

Station ID	Site Description[a]	Region Category	Periods Sampled	Latitude, Longitude	Depth (m)
2903	LACSD ocean outfall	Nearfield	All	33.698, −118.336	60
3053	LACSD off-outfall (northern current)	Nearfield	Summer 2014	33.730, −118.402	60
3003	LACSD off-outfall (northern current)	Nearfield	Spring 2015	33.757, −118.441	60
2803	LACSD off-outfall (southern current)	Nearfield	Summer 2015, Spring 2016	33.668, −118.297	60
2602	Long Beach Harbor Shelf (LA County)	Nearfield	All	33.694, −118.191	23
2205	OCSD ocean outfall	Nearfield	All	33.576, −118.005	57
2306	OCSD off-outfall (northern current)	Nearfield	Summer 2014	33.581, −118.052	114
2103	OCSD off-outfall (southern current)	Nearfield	Spring and Summer 2015, Spring 2016	33.585, −117.945	110
1903	Southern Transect Line (Orange County)	Nearfield	All	33.546, −117.836	100
CP1	Camp Pendleton (continental shelf)	Farfield	All	33.215, −117.481	65
CP2	Camp Pendleton (continental slope)	Farfield	All	33.184, −117.523	430
SPOTS	San Pedro Ocean Time Series (LA County offshore)	Farfield	All	33.607, −118.409	730
90.30	California Cooperative Oceanic Fisheries Investigations station 90.30 (Orange County offshore)	Farfield	All	33.419, −117.912	580

[a]Los Angeles (LA) County Sanitation Districts (LACSD) and Orange County Sanitation District (OCSD).

(OCSD) and Los Angeles (LA) County Sanitation District (LACSD) ocean outfalls, a nearshore farfield subregion off the coast of northern San Diego County (Camp Pendleton), and an offshore farfield subregion off the coast of LA and Orange counties (**Table 1**, **Figure 1**). Two stations were sampled in each subregion for the full suite of measurements and rate analyses. For the nearfield regions, sampling was dynamic and based on currents to enable sampling within the plume. A fixed sampling station was located directly over the outfall pipe, and a second site, which varied according to currents, was located a short distance from the outfall, but still within the plume. One additional fixed station was sampled in each effluent-plume subregion for water column nutrients and stable isotope analysis only (no rate data). For the farfield coastal subregion, one station was located on the continental shelf and the other on the shelf-break. For the offshore farfield subregion, one was located at the San Pedro Ocean Time Series station (offshore of the LACSD outfall) and the other at the California Cooperative Oceanic Fisheries Investigations (CalCOFI) sample station 90.30 (offshore of the OCSD outfall), both within the San Pedro Basin.

Comparisons and relationships were investigated seasonally, both when wastewater discharge was anticipated to constitute a minor fraction of the total N (TN) pool (spring upwelling period) and a major fraction (late summer, when the water column is stratified). Four seasons were sampled over 2 years: late summer stratification in 2014 and 2015, and spring upwelling in 2015 and 2016. Cruises and rate measurements were conducted over a 4-week period in each season, with one subregion sampled per week.

Sample collection

Vertical profiles were collected at each station using a Sea-Bird Electronics, Inc., SBE911plus (24 Hz) or SBE-25 (8 Hz) conductivity-temperature-depth (CTD) system, measuring a suite of oceanographic properties including pressure, temperature, salinity, CDOM, DO, pH, and chlorophyll fluorescence and transmissivity. In addition to the experimental stations, CTD casts were also taken at several stations in the nearfield subregions to map the location of the plume and regional hydrodynamics at the time of sampling (Figure S1). The profiles were averaged to 1-m bins. Regional climatologies of temperature, salinity, DO, chlorophyll *a*, and CDOM were generated by interpolation using the Barnes algorithm (Koch et al., 1983) from the R package "oce" (Kelley and Richards, 2017).

Discrete samples were collected from Niskin bottles (1.5 and 3 L) on a rosette deployed with the CTD sensor package. Sampling was adaptive at each site, with sample depths determined from downcast CTD observations to identify key oceanographic features at each station (CDOM to mark the plume, and the chlorophyll *a* maxima). Generally, samples were collected from 5 depths at the stations deeper than 50 m: the surface, subsurface chlorophyll maximum layer (depth of highest recorded chlorophyll fluorescence), the center of the thermocline (mixed layer, where the temperature gradient exceeds $-0.3°C\ m^{-1}$), below the thermocline, and at the "bottom" (2–5 m from the sediment surface or the end of the rosette cable, which was either 200 m at OCSD and LACSD stations or 300 m at Camp Pendleton stations). At shallower stations, 4 samples were collected from the surface,

subsurface chlorophyll maximum, the thermocline, and the bottom. For the nearfield subregions, the station over the outfall remained fixed throughout the study, but the second (off-outfall) nearfield station varied based on currents and was selected using CTD profiles of CDOM from several stations (Figure S1). CDOM has been shown to be a reasonable tracer for subsurface effluent plumes (Rogowski et al., 2012, 2013; Nezlin et al., 2020).

Field water samples were transferred from the Niskin bottles using acid-washed Tygon tubing into acid-washed 2-L high-density polyethylene (HDPE) bottles that were triple-rinsed with sample water before filling. Both LACSD and OCSD also supplied samples of effluent for analysis prior to each sampling event in their respective nearfield subregions. These samples were collected as a composite over 24 h in an acid-washed 1-L HDPE bottle. Effluent was stored at 4°C while the composite was generated.

Subsamples from both field water and effluent were collected for the suite of dissolved inorganic nutrients (nitrate + nitrite, nitrite, ammonium, and orthophosphate), total dissolved nitrogen and phosphorus, and dual nitrogen and oxygen isotope ratios for dissolved nitrate + nitrite. In addition, field water was subsampled for particulate organic matter concentrations (particulate nitrogen [PN], particulate phosphorus [PP], and particulate organic carbon), stable isotope ratios of carbon and nitrogen of particulate organic matter, and chlorophyll *a*. Subsamples were frozen immediately. Suspended particulate samples were collected by vacuum filtration onto precombusted (450°C for 4 h) glass fiber filters (Whatman GF/F). Suspended particulate samples were subsampled from the whole water sample for stable isotope analyses, filtered onboard the cruise, and frozen immediately. Filters were collected into snap-close Petri dishes and stored in Ziploc bags on ice in the dark for transport. Filters in the Petri dishes were dried at 50°C in the dark until analysis.

Subsamples for nutrient and stable isotope analyses were filtered by hand pump through a 0.45-µm polycarbonate filter (Millipore) and collected in triple-rinsed, 60-mL HDPE amber bottles, stored on ice for transport to the laboratory, and frozen until analysis (Wankel et al., 2006; Wankel et al., 2007; Santoro et al., 2010). Whole water for primary production and nitrification rate incubations were collected directly into acid-washed, triple-rinsed, 2-L HDPE bottles and stored on ice in the dark until the incubations could begin in the laboratory within 6 h of collection. Whole water for respiration rates was collected into 300-mL borosilicate glass biological oxygen demand bottles that were overfilled with twice the volume of the bottle. Water samples for the rate experiments (primary production, respiration, and nitrification) were stored on ice and in the dark until they were brought back to the lab for experimental preparation.

Laboratory analyses

Nutrient concentrations

Discrete samples were analyzed for a suite of dissolved nutrients. Nitrate + nitrite, nitrite, soluble reactive phosphate, and ammonium were analyzed using flow injection analyses (FIA, Lachat Instruments, QuikChem 8000 at the Marine Science Institute at the University of California, Santa Barbara), ammonium was also measured following the protocols of Holmes et al. (1999), TN and phosphorus samples were analyzed following persulfate digestion (Patton and Kryskalla, 2003) using FIA. A relative assessment of nutrient limitation, N*, was calculated, which represents the deviation in "Redfield" N:P stoichiometry due to additional sources and sinks of nitrate (Deutsch et al., 2001):

$$N^* = [NO_3-] - (16 * [PO_4{}^{3-}]) + 2.9. \quad (1)$$

Positive N^* values reflect regions with a source of new nitrate (via nitrogen fixation) and negative N^* reflects a sink of nitrate (due to denitrification). Values near zero are consistent with "Redfieldian" assimilation and nitrification of organic matter or that source and loss terms are balanced (Gruber and Sarmiento, 1997).

Stable isotope analyses

The stable isotopic compositions of dissolved nitrate + nitrite ($\delta^{15}N_{NO2+NO3}$ and $\delta^{18}O_{NO2+NO3}$), ammonium ($\delta^{15}N_{NH4}$), and suspended particulate matter ($\delta^{15}N_{PM}$ and $\delta^{13}C_{PM}$) are natural tracers of N sources and cycling in the ocean. Variation in the isotopic composition is attributable to distinct source signatures and the mass-dependent isotopic discriminations associated with various biogeochemical transformations that constitute the marine N cycle. Because each pathway causes a characteristic shift in isotope composition of the products and reactants, the isotopic composition of the dissolved and particulate pools can provide useful information on the mechanism of these transformations (Sigman et al., 2005; Wankel et al., 2007; Sugimoto et al., 2009).

The preparation and isotope analysis of $\delta^{15}N_{NO2+NO3}$ and $\delta^{18}O_{NO2+NO3}$ in discrete water samples was performed using a bacterial denitrification assay (Sigman et al., 2001; Casciotti et al., 2002). Samples with at least 0.002 mg kg^{-1} as N were analyzed by bacterial conversion of nitrate to nitrous oxide and subsequent measurement on a continuous flow isotope ratio mass spectrometer (Sigman et al., 2001; Casciotti et al., 2002; Coplen et al., 2012). Isotope ratios of $^{15}N/^{14}N$ and $^{18}O/^{16}O$ were measured using a ThermoFinnigan GasBench + PreCon trace gas concentration system interfaced to a ThermoScientific Delta V Plus isotope-ratio mass spectrometer at the Stable Isotope Laboratory at the University of California, Riverside. Dissolved ammonium was extracted from 250 mL of wastewater effluent onto glass fiber filter "traps" (Holmes et al., 1998; Hannon and Böhlke, 2008), and the isotope ratios of $^{15}N/^{14}N$ were measured using a coupled Costech Elemental Analyzer with a Finnigan Delta Plus Advantage in Continuous Flow Mode at the Stable Isotope Laboratory at the University of California, Riverside. The isotope ratios of $^{15}N/^{14}N$ and $^{13}C/^{12}C$ from suspended particulate matter collected on precombusted Whatman GF/F were also measured using the Costech instrument. Isotope ratios are reported relative to standards: N_2 in air for δ^{15} N, Vienna Standard Mean Ocean Water for $\delta^{18}O$, and Vienna Pee Dee Belemnite for $\delta^{13}C$. The standard deviation of replicate (*n*

= 20) standards for $\delta^{13}C_{PM}$ and $\delta^{15}N_{PM}$ was 0.084% and 0.165%, and the relative percent difference between measured standards and reference values was 0.32% and 0.88%, respectively. The standard deviation of replicate (n = 40) standards for $\delta^{18}O_{NO2+NO3}$ and $\delta^{15}N_{NO2+NO3}$ was 0.17% and 0.15%, and the relative percent difference between measured standards and reference values was 0.46% and 0.04%, respectively.

Rate measurements

Primary production rate measurements

Short-term incubations of natural plankton communities were conducted to determine rates of primary production, using radioactive ^{14}C-bicarbonate, with rates expressed as mg C m^{-3} day^{-1} or integrated vertically to units of mg C m^{-2} day^{-1}. Primary production was assessed at 4 depths bracketing the euphotic zone, from light levels of 95% to 1%: the surface (0–1 m), the center of the thermocline (5–50 m), the chlorophyll maximum (10–55 m), and the 1% light level (40–150 m; 3 times the Secchi depth). Depths were highly variable depending on season and distance from shore. Primary production was estimated from ^{14}C uptake using a simulated in situ technique in which the assimilation of dissolved inorganic carbon by phytoplankton yields a measure of the rate of photosynthetic primary production in the euphotic zone (Anderson et al., 2006; Brzezinski and Washburn, 2011).

Water was collected from Niskin bottles into 2-L HDPE bottles wrapped in black electrical tape and kept in darkened coolers until transported to the laboratory. Subsamples from each depth were separated into two acid-cleaned 250-mL polycarbonate bottles; one bottle was wrapped in black electrical tape to measure dark ^{14}C uptake, and the other was left open to light but darkened to expected ambient light levels using a neutral density screen. Bottles were incubated for 24 h after inoculation with ^{14}C-sodium bicarbonate in incubators placed outside in ambient light in the Southern California Coastal Water Research Project facility, held at recorded in situ seawater temperatures by circulating incubator water through chillers. At the end of incubations, total radioactivity in each sample was determined by adding 250 µL of incubated seawater to 250 µL of β-phenethylamine in a 20-mL glass scintillation vial followed by 10 mL of Ultima Gold XR scintillation cocktail. Each vial was shaken vigorously for 30s and ^{14}C activity assayed after bubbles had cleared and chemoluminescence had subsided (approximately 2 h) by a liquid scintillation counter using an internal quench curve. A 50-mL subsample of incubated water was also filtered through a precombusted 25-mm Whatman GF/F filter. Filters were placed in individual 20-mL glass scintillation vials and 0.25 mL of 0.5 N HCl was pipetted onto each filter in a fume hood to drive off excess tracer. Vials were left uncapped for a minimum of 7 h, and 10 mL of Ultima Gold XR scintillation cocktail was added to each vial, the vials capped and shaken, and ^{14}C activity was analyzed by scintillation counter using an internal quench curve. Primary productivity rates in both the light and dark incubations were calculated as described by Anderson et al. (2006) and Brzezinski and Washburn (2011). Daily primary production (g C m^{-3} d^{-1}) was calculated as the difference in productivity between light and dark bottles. Productivity-to-biomass ratio was calculated as the daily primary productivity (g C m^{-3} d^{-1}) per unit chlorophyll *a* (g chl a m^{-3}) with units of g C (g chl a)$^{-1}$ d^{-1}. Depth-integrated rates of productivity were calculated using the trapezoidal method.

Respiration rate measurements

Respiration rates were measured at 4 depths: the chlorophyll maximum (10–55 m), the middle of the thermocline (5–50 m), below the thermocline (40–150 m), and 2–5 m above the seabed or at the end of the CTD cable (see above). Specific depths varied depending on season and distance from shore. Whole water was collected from Niskin bottles into 300-mL glass bottles, each of which was wrapped in black electrical tape, using acid-cleaned Tygon tubing, overfilling each bottle with at least twice the volume. Three bottles were collected for respiration rate measurements at each depth. An additional 50-mL syringe of whole water was collected from each Niskin bottle and held in a cooler. An initial DO concentration (mg O_2 L^{-1}) and percent oxygen saturation were recorded in the field for each bottle using a YSI ProDO optical DO probe, immediately after bottles were filled. Because the probe displaced some water from each bottle, water was replaced with whole water from the syringe to eliminate headspace in each bottle. Bottles were then stoppered and placed in refrigerated units held at in situ water temperatures. Bottles were incubated for 24–48 h and final DO concentration (mg O_2 L^{-1}) and percent oxygen saturation in each bottle were recorded. Respiration rates were calculated for each depth at in situ temperatures as the difference between time-zero oxygen concentrations and final incubated oxygen concentrations.

Nitrification rate measurements

Nitrification is the sequential oxidation of NH_4^+ to NO_3^- via NO_2^-. Nitrification rates were determined by measuring the accumulation of ^{15}N in the dissolved nitrate + nitrite pool following the addition of isotopically enriched ammonium to bottle incubations (Santoro et al., 2010). Water was collected from Niskin bottles into 2-L HDPE bottles at the same 4 depths selected for respiration rate measurements: the chlorophyll maximum layer, the middle of the thermocline, below the thermocline, and 2–5 m above the bottom or at the end of the CTD cable (see above). Subsamples from this initial sample were separated into three 500-mL acid-washed polycarbonate bottles wrapped in black tape. An enriched (99%) tracer of ^{15}N-ammonium chloride was added to 2 of the bottles to a final concentration of 100 nM, and a third bottle without the tracer served as a control. Not knowing ammonium concentrations beforehand, we targeted this concentration to minimize impact on nitrogen cycling within the bottles. The percentage of labeled ammonium ranged from 0.01 to 1.5%, with a median value of 0.1%. Bottles were incubated in the dark, to minimize N uptake by phytoplankton, and as close to in situ temperature conditions as possible (within ± 2°C) in a series of

Table 2. Nutrient properties of Los Angeles County Sanitation District (LACSD) and Orange County Sanitation District (OCSD) wastewater effluent during the study period. DOI: https://doi.org/10.1525/elementa.2020.00145.t2

	LACSD				OCSD			
Property	August 2014	March 2015	August 2015	March 2016	August 2014	March 2015	August 2015	March 2016
Discharge rate (MGD)	268	263	257	256	125	119	92	93
PO_4 (μM)	5.5	5.3	3.8	3.5	23.4	34.6	26.5	24.2
NO_2 (μM)	3.9	6.1	15.1	6.2	196	238	152	170
NO_3 (μM)	5.1	4.2	10.5	6.5	883	852	784	850
NH_4 (μM)	2,690	3,460	2,670	1,260	1,890	1,460	1,800	2,990
DIN (μM)	2,700	3,470	2,700	1,270	2,970	2,550	2,740	4,010
DIN loading (g day^{-1})	3.8×10^7	4.8×10^7	3.7×10^7	1.7×10^7	1.9×10^7	1.6×10^7	1.3×10^7	2.0×10^7
N:P	490	652	1540	852	127	74	103	94
DOC (μM)	1,110	1,170	1,380	1,920	1,190	1,130	1,500	2,240
DIC (μM)	4,900	na	4,360	2,750	5,080	6,400	4,400	2,910
$\delta^{15}N_{NO2+NO3}$ (‰)	−9.6	−2.3	na	na	9.1	7.5	na	na
$\delta^{18}O_{NO2+NO3}$ (‰)	−15.2	−15.6	na	na	−5.8	−3.5	na	na
$\delta^{15}N_{NH4}$ (‰)	7.5	5.1	9.6	12.4	9.1	8.9	8.6	9.1

na = not analyzed; DIN = dissolved inorganic nitrogen; MGD = million gallons per day; DOC = dissolved organic carbon; DIC = dissolved inorganic carbon.

refrigerated incubator units. For reference, Q_{10} values for nitrification are on the order of 2–3 (Henriksen and Kemp, 1988). Subsamples of 50 mL each were collected at 4 time points (approximately 0, 12, 24, and 36 h post spike addition), syringe-filtered through 0.45-μm filters and frozen until analysis for dissolved nitrate + nitrite concentration and $\delta^{15}N_{NO2+NO3}$ as described above. Potential nitrification rates were determined by modeling the ^{15}N and ^{14}N contents of the nitrate + nitrite pool with inputs from the labeled ammonium pool and outputs through nitrate + nitrite uptake as described in Santoro et al. (2010). Data-fitting for the ^{15}N and ^{14}N values measured at each time point was performed by nonlinear least squares regression method using MATLAB 8.2 and Statistics Toolbox 8.3 (The MathWorks, Inc.).

Statistical analysis

To understand relationships between state variables and rates, we employed several statistical techniques: analysis of variance (ANOVA), Kruskal–Wallis (when ANOVA assumptions failed), Spearman Rank, and Random Forest regression. To characterize relationships between variables, we used ANOVA for normally distributed data and Kruskal–Wallis and Spearman Rank for nonparametric measures of rank correlation using the R packages (R Core Team, 2019) "Tidyverse," Wickham et al., 2019) and "Hmisc" (Harrell, 2014). We used Random Forest modeling to characterize variable importance in constraining the variance of rate measurements. Random forest modeling, a machine-learning statistical method that combines many classification trees to produce a more accurate classification (Breiman, 2001; Cutler et al., 2007), has been found to be a robust tool for interpreting ecological data sets (Prasad et al., 2006; Cutler et al., 2007). Random forests provide several metrics that aid in interpretation of multivariable data sets. Variable importance can be evaluated based on how much worse the prediction would be if the data for that predictor were permuted randomly. The resulting tables can be used to compare relative importance among predictor variables (Prasad et al., 2006). Random Forests were conducted using the R package "randomForest" (Liaw and Weiner, 2012).

Results

Wastewater effluent characterization

Throughout the study period, the effluent nutrient concentrations, isotope ratios, and discharge rates at each outfall were slightly variable (**Table 2**). Over this period, both the LACSD and OCSD effluent discharge rates decreased slightly, as part of a long-term trend related to increasing water use efficiency and reduced water consumption in California. During this same time, LACSD (2014, 2015, 2016) discharged an average ($\pm$ standard deviation, $n = 730$) of 4.1×10^7 ($\pm$ 4.5×10^6) grams of dissolved inorganic nitrogen (DIN) per day and OCSD (2015, 2016) an average of 1.5×10^7 ($\pm 3.2 \times 10^6$) grams of inorganic nitrogen per day. The characteristics of effluent from OCSD and LACSD were different, likely due to differences in their treatment systems. OCSD wastewater treatment is secondary with advanced nitrification/denitrification, while LACSD has secondary treatment with no advanced nutrient removal. Ammonium accounted for

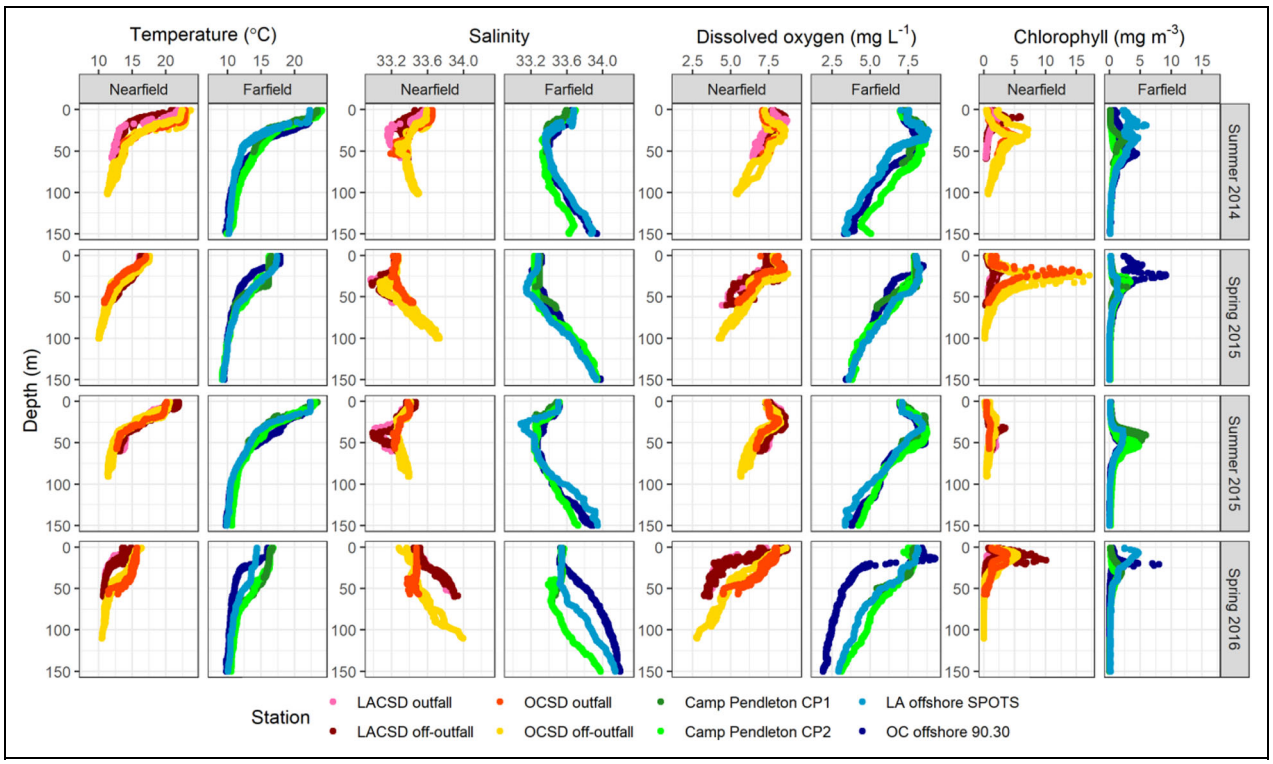

Figure 2. Spatial and temporal patterns in temperature, salinity, dissolved oxygen, and chlorophyll during each sampling event. Figure is faceted by nearfield and farfield stations (as defined and located in **Figure 1**) for each parameter and by season; colors represent the stations. Each subregion was sampled in a different week in a single month, introducing some temporal variability into the data set within a season. The outfall plumes were generally located between depths of 20 and 60 m at the nearfield sites (Figure S1). DOI: https://doi.org/10.1525/elementa.2020.00145.f2

>99% of the LACSD DIN load and between 55% and 67% of the OCSD DIN load. The OCSD effluent contained more phosphate compared to LACSD, with an average N:P molar ratio of 100:1 for OCSD and 678:1 for LACSD (**Table 2**). Dissolved inorganic carbon and dissolved organic carbon were highly variable in both agency effluents throughout the study period. The stable N isotopic composition of ammonium and nitrate + nitrite was different for both treatment plants. OCSD had relatively consistent values for $\delta^{15}N_{NH4}$, ranging between 8.6% and 9.1%, and $\delta^{15}N_{NO2+NO3}$, ranging between 7.5% and 9.1%, while LACSD had $\delta^{15}N_{NH4}$ values ranging from 5.1% to 12.4% and $\delta^{15}N_{NO2+NO3}$ values ranging between −9.6% and −2.3%. The ammonium isotopic composition in the LACSD effluent was related linearly to the concentration of ammonium in the wastewater (for LACSD, $r^2 = .907$, $P = 0.04$; for OCSD, $r^2 = .364$, $P = 0.505$).

Seasonal hydrography, chlorophyll, and DO

Clear seasonal differences in temperature and salinity were observed throughout the study region (**Figures 2** and S2). Summer surveys were characterized by high surface water temperatures, shallow thermoclines and haloclines (at approximately 10–15 m), and steep vertical temperature gradients, indicating strong thermal stratification. Spring surveys were characterized by weaker vertical thermal gradients and deeper thermoclines and haloclines (at approximately 20–30 m). The wastewater plume was identifiable by both low salinity and high CDOM in both the LACSD and OCSD nearfield subregions at mid-depth. During spring 2016, a cold, high salinity, low DO water mass was intruding into the region from depth throughout the Palos Verdes Shelf region and notably in the Orange County offshore station (CalCOFI station 90.30; **Figure 1**).

No statistically significant differences were observed between DO in nearfield versus farfield areas (Kruskal–Wallis). Nearfield stations generally had shallower oxyclines compared to farfield stations, but that is likely due to their proximity to shore compared to most farfield stations, except for CP1 (**Figure 2**). DO profiles varied seasonally (**Figures 2** and S2). In the summer, all regions had similar profiles and a narrower range of values in the upper 60 m. During the spring surveys, DO had a larger range of values in the upper 60 m, with surface ocean values similar to summer, but much lower at depth. Spring also had greater variability in the depth to the oxycline among different stations. The lowest DO was in deeper waters and shoaled closer to the surface during spring (particularly spring 2016), indicative of upwelling of cold, deep waters, low in DO.

Chlorophyll fluorescence in nearfield areas was slightly, but significantly, higher than in farfield areas within the first 60 m of the water column, which captures the depth of the chlorophyll maximum at all stations, with a mean chlorophyll *a* concentration of 2 μg L^{-1} in the nearfield compared to 1 μg L^{-1} in the farfield ($P < 2e^{-16}$). Daytime

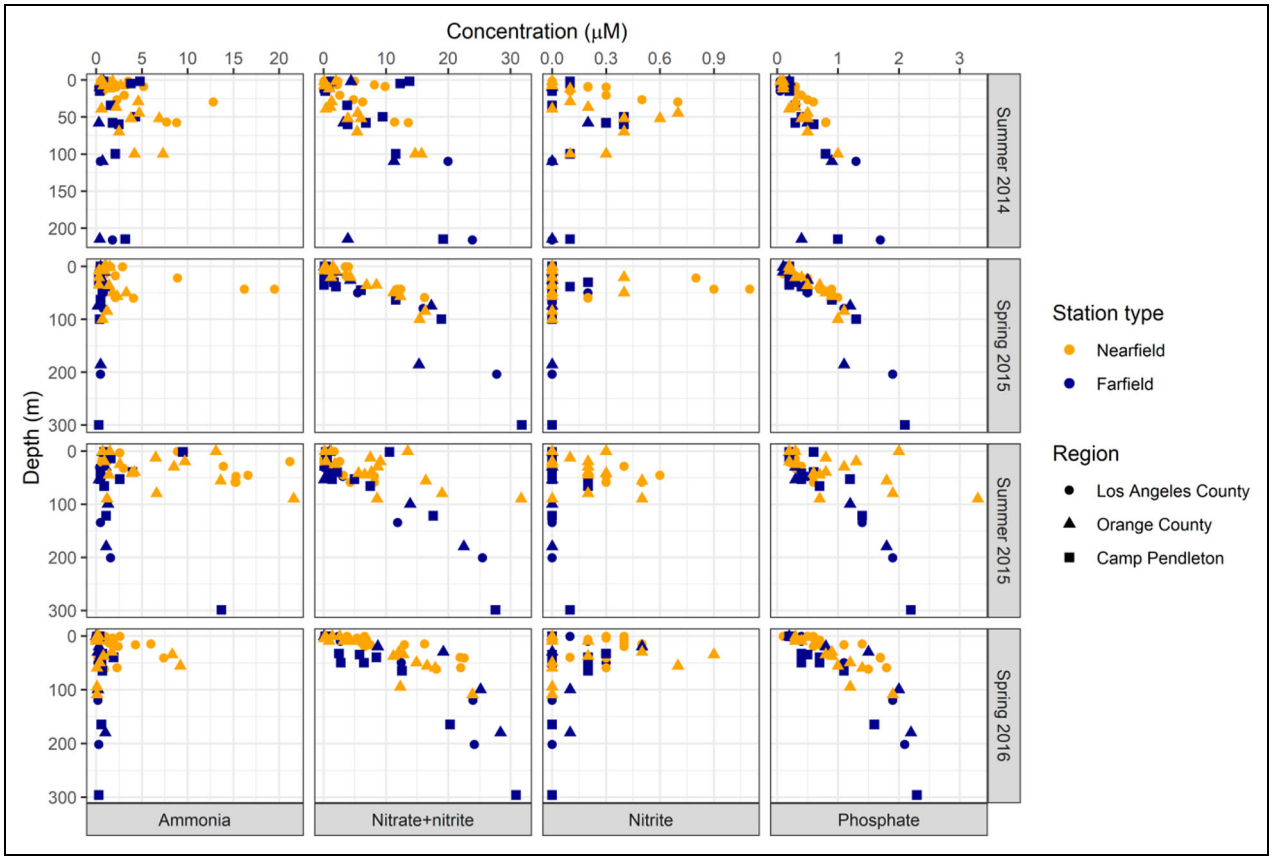

Figure 3. Depth profiles of the dissolved inorganic nutrients ammonium, nitrate + nitrite, nitrite, and phosphate. Colors represent the station types; shapes represent the regions. The outfall plumes were generally located at depths between 20 and 60 m in the nearfield sites (Figure S1). DOI: https://doi.org/10.1525/elementa.2020.00145.f3

chlorophyll florescence had a similar vertical structure to DO, with a clear subsurface maximum layer in all seasons (**Figure 2**). The depth to and magnitude of the subsurface chlorophyll maximum was variable among stations and among seasons. The lowest chlorophyll was during summer 2015 and the highest during spring 2015. The highest values during spring 2015 were associated with the LACSD and OCSD nearfield areas, appearing as a thin subsurface chlorophyll layer (**Figure 2**). Spring 2016 had a shallow, narrow chlorophyll layer, with no chlorophyll fluorescence associated with the deep, salty water mass present in spring 2016. Summer 2014 had middling water column chlorophyll that was deeper offshore and shallower nearshore, whereas summer 2015 had relatively low chlorophyll overall with the most consistency among stations.

Sampling occurred over a 4-week period for each season, which may have introduced some variability among stations; however, there was no clear pattern within any sampling season of the nearfield stations showing consistently different hydrographic conditions relative to the farfield stations that might create bias in the data set (Figure S2).

Water column nutrient concentrations

Dissolved inorganic nutrients

Despite the continuous N-loading from both wastewater treatment plants, concentrations of DIN in surface waters were generally low in all subregions (**Figure 3**), but not completely depleted. Surface DIN values ranged from not-detected to 26.9 μM with a mean value of 3.6 μM in farfield areas and 4.7 μM in nearfield areas. Nutrient profiles generally showed lower concentrations in surface waters with increasing concentrations at depth (**Figure 3**). Mean DIN concentrations for samples collected below the thermocline ranged from 0.6 to 53.9 μM, with a mean value of 18.7 μM in farfield areas and 17.0 μM in nearfield areas. Excluding the bottom sample (which was collected at greater depths offshore compared to the nearshore sites), ammonium and nitrite were significantly higher in the nearfield stations compared to farfield, nonplume stations (P values of 0.000542 and $1.30e^{-5}$, respectively). High concentrations of ammonium (maximum value of 18.8 μM, mean value of 5 μM) and nitrite (maximum value of 1.1 μM, mean value of 0.4 μM) were associated with the plume mixing zone (as detected by CDOM; Figure S1) in the nearfield regions, the depth where the plume reaches neutral buoyancy in the water column (between 20 and 60 m). Nitrate + nitrite and phosphate were not significantly different in the nearfield compared to the farfield. All dissolved inorganic nutrients showed significant differences by season ($P = 3.86e^{-6}$ for nitrate + nitrite, $P = 7.69e^{-5}$ for ammonium, and $P = 1.03e^{-10}$ for phosphate), except for nitrite ($P = 0.15$).

Suspended particulate nutrients

Particulate nutrients suspended in the water column had similar profiles, with the highest concentrations at the

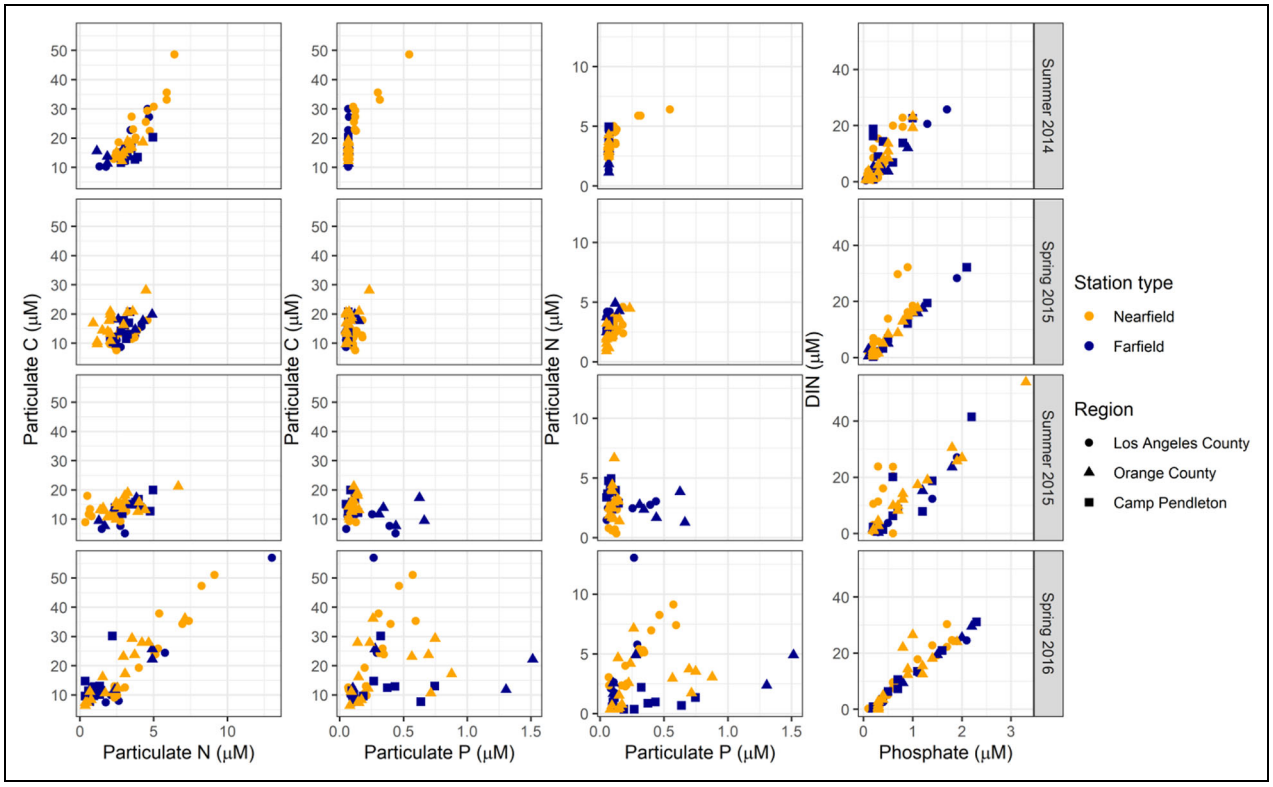

Figure 4. Property-property plots for dissolved and particulate nutrients. Particulate carbon as a function of particulate nitrogen and particulate phosphorus (left columns), particulate nitrogen as a function of particulate phosphorus (third column), and dissolved inorganic nitrogen (DIN) as a function of dissolved phosphate (right column). Colors represent the station types; shapes represent the regions. DOI: https://doi.org/10.1525/elementa.2020.00145.f4

surface decreasing with depth (Figure S3). Mean values for PN were 3.5 μM at the surface and 2.5 μM below the thermocline; for PP, 0.18 μM at the surface and 0.12 μM below the thermocline; and for particulate carbon (PC), 19.0 μM in the surface and 13.2 μM below the thermocline. No statistically significant differences were observed by station type for PN or PP, but PC was slightly, significantly higher in nearfield stations (Kruskal–Wallis, $P = 0.03$), particularly those within the plume mixing zone as detected by CDOM (with mean PC concentrations of 21 μM for depths within the plume in nearfield stations compared to 16.9 μM for similar depths in farfield stations). Significant differences were also observed by season for all particulate parameters (Kruskal–Wallis, $P = 0.0008$, 0.02, $2.2e^{-16}$, for PC, PN and PP, respectively). Spring 2016 was slightly anomalous from the other three seasons, exhibiting higher concentrations in PC, PN, and PP in surface samples relative to the other seasons, perhaps related to the cold, salty water mass intrusion during that season.

Nutrient ratios

Nutrient concentrations for particulate matter and dissolved inorganic nutrients were highly correlated, following the Redfield relationship of C:N:P 106:16:1 (**Figures 4** and S4). The mean N:P ratio for dissolved nutrients (DIN:P) was 15.4 and was significantly lower ($P = 0.028$) in the farfield (mean of 13.4) compared to the nearfield (mean of 17.5). The highest mean DIN:P ratios were in the nearfield stations at depths associated with the plume (mean of 18.5). The lowest mean DIN:P ratios were recorded at the chlorophyll maximum depth in the farfield (mean of 9.9). N* showed strong seasonality, with water column values close to 0 during the spring upwelling periods, whereas the summer fluctuated between positive N* values (summer 2014), indicative of a source of nitrate, and negative N* values (summer 2015), indicative of a sink for nitrate (**Figures 5** and S5). N* values near zero suggest that there were no large sources of new nitrate (e.g., from nitrogen fixation) or sinks (e.g., due to denitrification).

PN and PC were highly correlated, with 90% of C:N ratios falling between 3.8 and 20.0 and a mean regional C:N ratio of 6.7. Some differences were observed between particulate C:N ratios in the nearfield and farfield (with mean values of 7.1 and 6.3, respectively). C:N ratios less than 6 were found throughout the water column and are atypical of phytoplankton and often associated with bacteria (Goldman et al., 1987). C:P and N:P relationships were close to Redfield, with occasional deviations. These deviations were not related to depth (Figure S4) and were more closely tied to station type, with nearshore stations (nearfield stations and farfield, coastal stations at Camp Pendleton) having greater variability than farfield, offshore stations. Relatively high PP concentrations were not matched by similarly high concentrations in PN and PC during spring 2016.

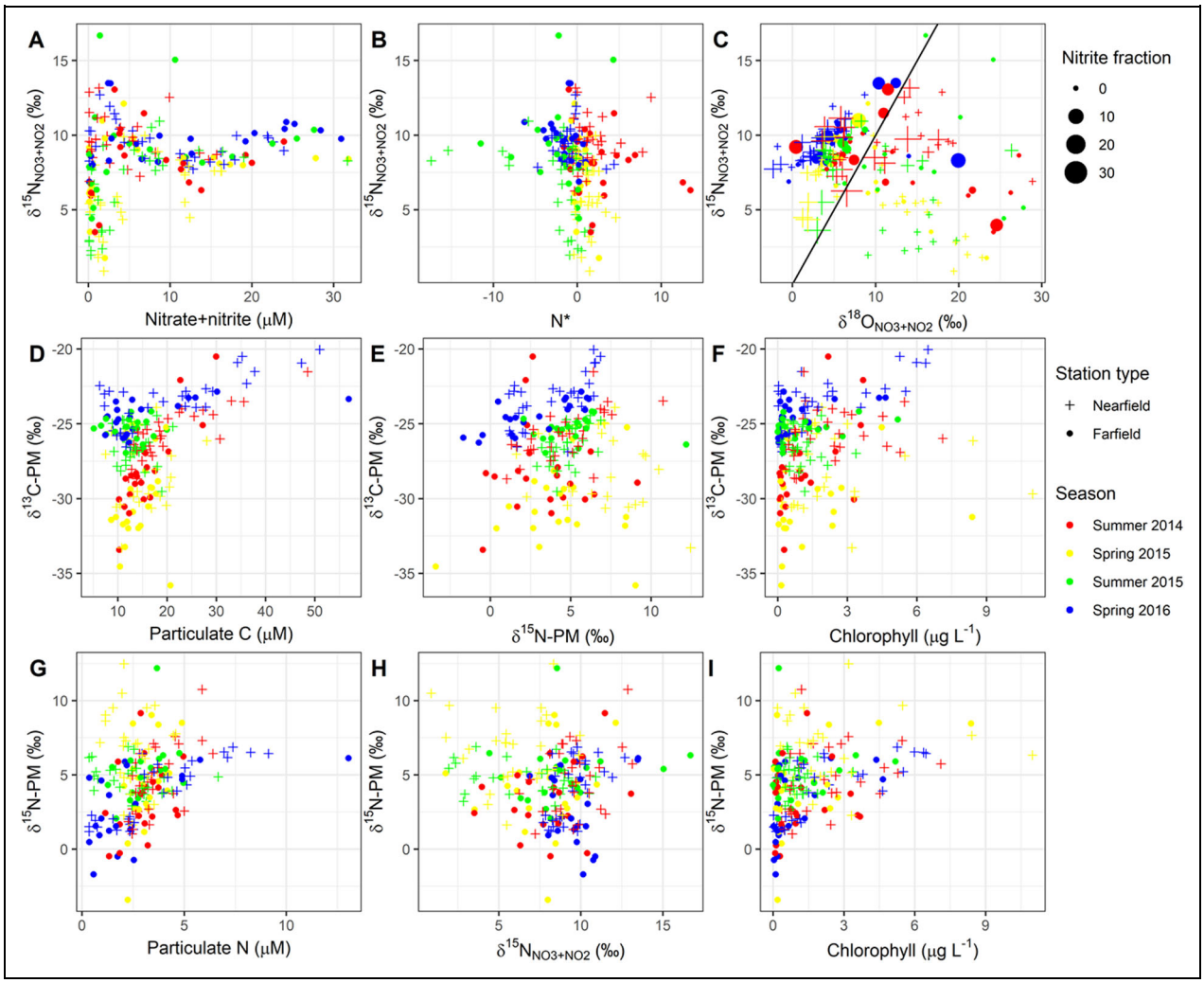

Figure 5. Property-property plots of stable isotope data and nutrient and chlorophyll concentrations. (A) $\delta^{15}N_{NO3+NO2}$ and nitrate + nitrite concentration; (B) $\delta^{15}N_{NO2+NO3}$ and N*; (C) $\delta^{15}N_{NO2+NO3}$ and $\delta^{18}O_{NO2+NO3}$, where the black line represents 1:1; (D) $\delta^{13}C_{PM}$ and particulate carbon concentration; (E) $\delta^{13}C_{PM}$ and $\delta^{15}N_{PM}$; (F) $\delta^{13}C_{PM}$ and chlorophyll *a*; (G) $\delta^{15}N_{PM}$ and particulate nitrogen concentration; (H) $\delta^{15}N_{PM}$ and $\delta^{15}N_{NO2+NO3}$; and (I) $\delta^{15}N_{PM}$ and chlorophyll *a*. Shapes represent the station types; colors represent the season. The size of the points only applies to the nitrite fraction in panel (C) where an increased nitrite fraction in nitrite + nitrate may underestimate $\delta^{18}O_{NO2+NO3}$. See text and Figure S12 for how this underestimation may affect results. DOI: https://doi.org/10.1525/elementa.2020.00145.f5

Water column isotope ratios

Stable isotopic composition of dissolved nitrate + nitrite

$\delta^{15}N_{NO2+NO3}$ values were generally lower in surface waters (mean of 7.5‰), increased to a subsurface maximum (mean of 9.5‰), before decreasing again (to mean of 8.7‰). $\delta^{15}N_{NO2+NO3}$ was significantly higher in the farfield, nonplume stations compared to nearfield stations ($P = 0.02$). The $\delta^{18}O_{NO2+NO3}$ was highest in surface waters (mean of 14.6‰) and decreased with depth (mean of 5.2‰) with no obvious maximum or minimum (**Figure 6**). The shapes of profiles for both $\delta^{15}N_{NO2+NO3}$ and $\delta^{18}O_{NO2+NO3}$ corresponded with the vertical distribution of nitrate + nitrite, DO, and chlorophyll. There were also significant differences in $\delta^{15}N_{NO2+NO3}$ and $\delta^{18}O_{NO2+NO3}$ values between sampling seasons (*P* values of $3.07e^{-10}$ and $6.99e^{-9}$, respectively).

At low nitrate + nitrite concentrations, $\delta^{15}N_{NO2+NO3}$ values were variable but approach values between 7 and 9‰ for all sampling periods as the concentration of nitrate + nitrite, the fraction of nitrite in the DIN pool, and the nitrification rate all increase (**Figures 5** and S5), similar to what has been seen in urban coastal environments (Sugimoto et al., 2009; McLaughlin et al., 2017). There was no significant relationship between $\delta^{15}N_{NO2+NO3}$ and N*, largely because N* was typically very close to zero for most sampling stations and events (**Figures 5B** and S5).

Stable isotopic composition of suspended particulate matter

The stable C and N isotopic compositions of suspended particulate matter ($\delta^{13}C_{PM}$ and $\delta^{15}N_{PM}$) were lower at the surface (–25.9‰ and 4.6‰, respectively), increased to a subsurface maximum (–25.5‰ and 5.4‰, respectively)

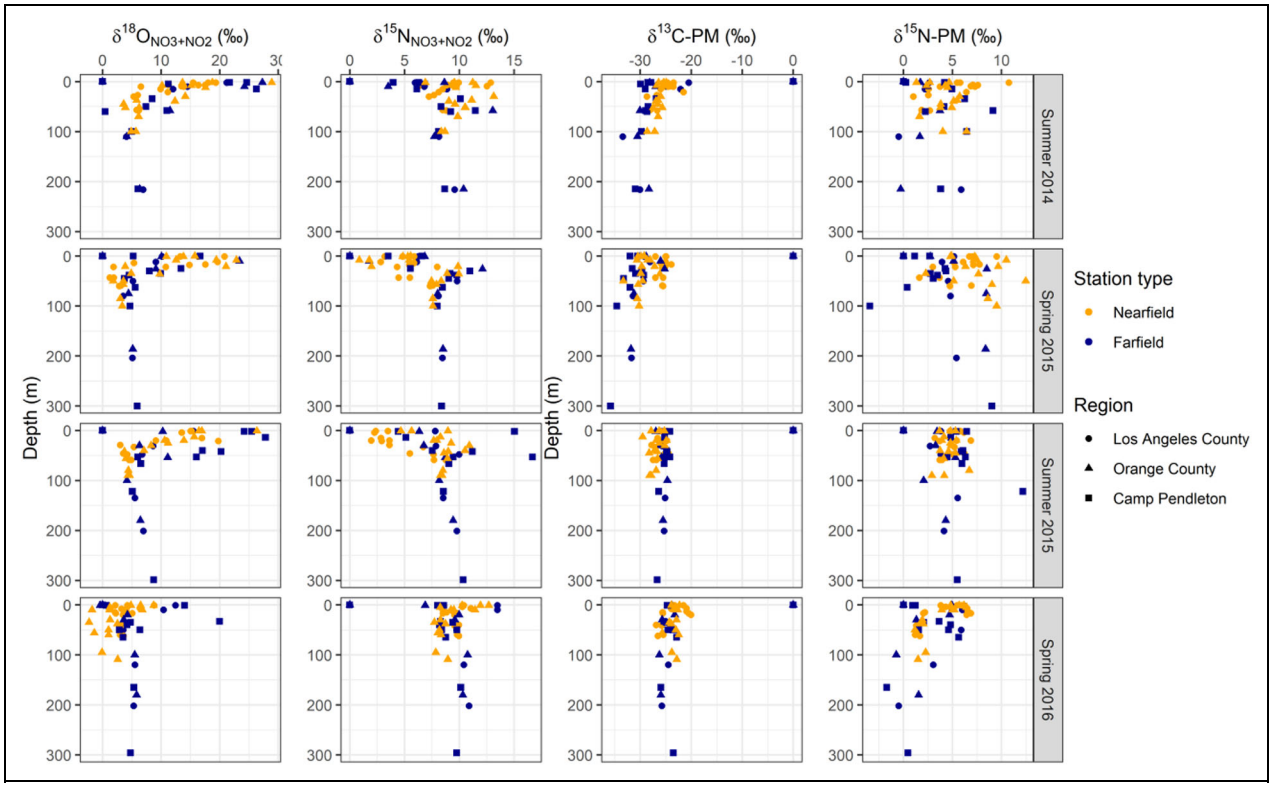

Figure 6. Depth profiles of dissolved $\delta^{15}N_{NO3}$ and $\delta^{18}O_{NO3}$ and particulate $\delta^{13}C_{PM}$ and $\delta^{15}N_{PM}$. Colors represent the station types; shapes represent the regions. The outfall plumes were generally located between depths of 20 and 60 m in the nearfield sites (Figure S1). DOI: https://doi.org/10.1525/elementa.2020.00145.f6

and then decreased at depth (–27.2‰ and 4.2‰, respectively; **Figures 6** and S6). Both $\delta^{13}C_{PM}$ and $\delta^{15}N_{PM}$ were significantly higher in the nearfield areas relative to the farfield ($P = 1.68e^{-06}$ and .00107, respectively). There were also significant temporal differences in $\delta^{13}C_{PM}$ and $\delta^{15}N_{PM}$ ($P < 2e^{-16}$ and $P = 8.22e^{-06}$, respectively). Mean values for $\delta^{13}C_{PM}$ in summer 2014 (–26.7‰) and spring 2015 (–28.9‰) were lower than in summer 2015 (–26.0‰) and spring 2016 (–23.8‰), while the mean value for $\delta^{15}N_{PM}$ was highest in spring 2015 (5.7‰) and lowest in spring 2016 (3.4‰), with both summer periods having similar mean values (4.4‰ in summer 2014; 4.9‰ in summer 2015; **Figures 6** and S6). $\delta^{15}N_{PM}$ showed an asymptote to values between 4‰ and 10‰ with increasing particulate N concentration and chlorophyll *a* concentration (**Figures 5I** and S7). By contrast, no significant relationship between $\delta^{15}N_{PM}$ and particulate N or $\delta^{15}N_{NO2+NO3}$ was observed (**Figures 5G**, **H**, and S7). $\delta^{13}C_{PM}$ also correlated positively with $\delta^{15}N_{PM}$ for most stations and seasons and showed an asymptote between –26‰ and –20‰ with increasing PC concentration and chlorophyll *a* (**Figures 5F** and S8). $\delta^{13}C_{PM}$ correlated negatively with water column DIN (Figure S8).

Primary production and respiration

Large spatial/temporal variability was observed in rates of both primary production and respiration (**Figures 7A**, **B**, and S9). Primary production rates ranged from 129 to 2,840 mg C m^{-2} d^{-1}, and respiration rates ranged from 80.6 to 1520 mg O_2 m^{-3} d^{-1}. Seasonality in primary production was evident for the two farfield offshore stations, with higher production during spring, likely due to upwelling, compared to summer. However, for the nearshore stations (nearfield stations and the farfield, coastal stations at Camp Pendleton), there were no statistically significant differences in primary production between season or station type (nearfield vs. farfield; Figure S9). Similarly, respiration rates offshore were typically higher than nearshore values, but there were no significant differences between the nearfield stations and farfield, coastal stations (**Figure 7B**). Primary productivity values were similar to those reported previously for the region (Smith et al., 1982; Eppley, 1992) with similar seasonality (Mantyla et al., 2008). Respiration rates are within the range of other coastal areas and slightly higher than those reported for the Pacific coastal environment (Robinson, 2019), with no significant differences between the LACSD and OCSD nearfield sites (Figure S9). There was no significant relationship between primary production and respiration for any season (Figure S10). Sample sizes for assessing such relationships, however, were small, with only one depth-integrated rate for both primary production and respiration per station ($n = 12$ for nearfield and farfield sites, 24 total primary production rate estimates; $n = 16$ for nearfield and farfield sites, 32 total respiration rate estimates).

Nitrification

Nitrification rates were highly variable throughout the study, ranging from 0.001 to 325 nmol L^{-1} day^{-1}, with no clear seasonal patterns. Rates were significantly higher

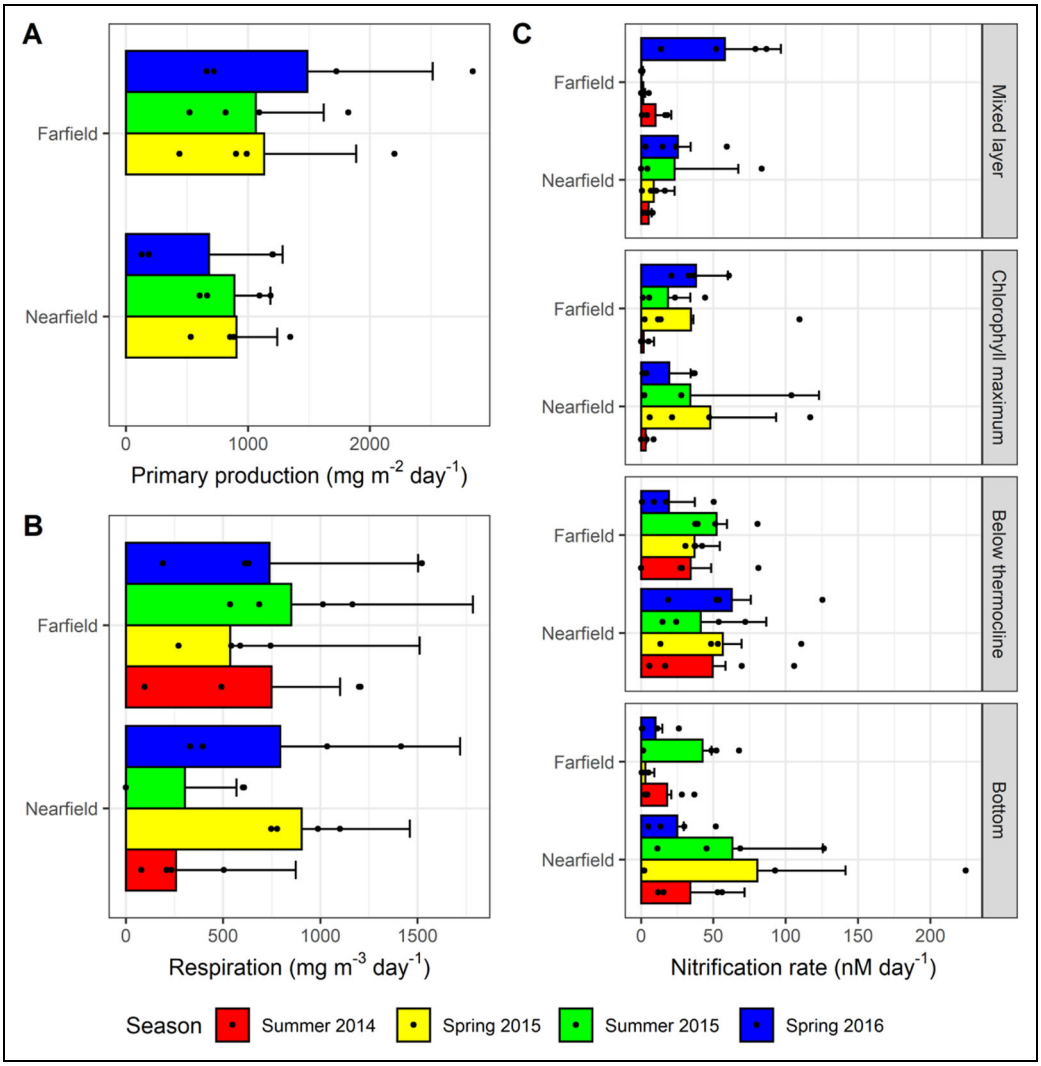

Figure 7. Depth-integrated primary production, average subsurface respiration, and depth-layer nitrification rates by station type and season. (A) Depth-integrated (photic zone, 0–60 m) primary production rates (no data collected in summer 2014); (B) average respiration rates (for the water column); and (C) nitrification rates by depth layer. Black points represent individual data points. Error bars indicate standard deviation. DOI: https://doi.org/10.1525/elementa.2020.00145.f7

in samples collected below the thermocline (mean of 40.0 nmol L^{-1} day^{-1}) compared to samples collected in the mixed layer (16.5 nmol L^{-1} day^{-1}) and deep chlorophyll *a* maximum (24.6 nmol L^{-1} day^{-1}; $P = 0.01$; **Figure 7C**), similar to profiles measured by others (Ward, 1987, 2005; Santoro et al., 2010; Smith et al., 2014) and attributed to light inhibition of nitrification in surface waters. Rates were highest in nearshore stations (mean of 35.2 nmol L^{-1} day^{-1} in the nearfield stations and the farfield, coastal stations at Camp Pendleton) compared to the two offshore stations (mean of 21.1 nmol L^{-1} day^{-1} offshore) and were significantly higher in nearfield areas (36.2 nmol L^{-1} day^{-1}) relative to farfield areas (23.6 nmol L^{-1} day^{-1}; $P = 0.04$). There were no significant differences between LACSD and OCSD nearfield stations (Figure S9).

Discussion

Anthropogenic nutrient discharges into coastal waters can drive significant biogeochemical changes, and local managers are being urged to consider whether nutrient management strategies can slow the progression of acidification and deoxygenation and their impacts on coastal habitats (Kelly et al., 2011; Strong et al., 2014; Chan et al., 2016). Globally, wastewater discharge, 80% of which is untreated (United Nations World Water Assessment Programme, 2017), represents a significant pathway of nutrient enrichment and eutrophication of coastal waters. However, the relative impact of these inputs compared to global change on N and C biogeochemical cycling is poorly characterized (Kelly et al., 2011; Strong et al., 2014), particularly in the eastern boundary upwelling system of this study. We documented that wastewater nutrient inputs may have an immediate, local effect on nutrient stoichiometry, elevating ammonium and nitrite concentrations and increasing dissolved N:P ratios, as well as increasing rates of nitrification within the plume and slightly increasing chlorophyll *a* concentrations. We did not observe a consistent, near plume effect on primary production, respiration, or DO, suggesting that any potential impact from wastewater on these processes might be

moderated by regional factors, notably mixing of water masses. Furthermore, a regional assessment of aragonite saturation state conducted at the same time as this study, indicated that there was no clear pattern of reduced saturation state near ocean outfalls (McLaughlin et al., 2018). These findings suggest that further study of implications of wastewater nutrients on the lower trophic ecosystem of the SCB through ocean numerical modeling studies is warranted, given the difficulty in disentangling local versus regional versus global drivers through observations alone.

The impacts of anthropogenic nutrient inputs on the biogeochemical cycling of nitrogen in the immediate vicinity of outfalls

The doubling of coastal ocean annual nitrogen loads from wastewater outfalls (Howard et al., 2014) has important implications for nitrogen cycling in the nearshore. Wastewater nitrogen appears to be altering the composition of the N pool within the plumes; ammonium and nitrite concentrations were elevated in the nearfield regions compared to farfield regions (**Figure 3**). Furthermore, the absence of seasonal difference in nitrite concentration suggests a source of nitrite independent of seasonal upwelling.

The N:P ratio in coastal waters also appears to be altered by the presence of wastewater plumes. The ratio of N:P is a nearly constant 16:1 throughout the world's oceans, in both plankton biomass and dissolved nutrient pools (Redfield, 1958), and the farfield stations adhere closely to this ratio (**Figure 4**). However, the nearfield stations had elevated N:P ratios, which can be attributed to the relatively low concentrations of P compared to N in wastewater effluent (N:P of 115:1; **Table 2**). This increase in P-limitation near outfalls may have important implications for the planktonic community compositions near these discharges (Grosse et al., 2017; Moreno and Martiny, 2018; Fagan et al., 2019). For example, P-limitation has been linked to increased toxin production in *Pseudo-nitzschia* (Fehling et al., 2004), a common harmful algal bloom species in the SCB (Schnetzer et al., 2007; Smith et al., 2018).

Nitrification of ammonium to nitrate plays an important role in coastal ocean nitrogen cycling (Ward, 1987, 2005) and can support a significant fraction of productivity in surface waters (Wankel et al., 2007; Santoro et al., 2010). Nitrification rates were significantly higher in nearfield stations compared to farfield areas, suggesting that the ammonium from wastewaters may be increasing these rates within the plumes. As the high concentrations of ammonium in the nearfield and the relatively small percentage of labeled ammonium added to these samples during the incubation experiments (less than 1% spike) may have resulted in an underestimation of nitrification in the nearfield samples, the differences in nitrification rates in the nearfield compared to the farfield may be even greater than what is described here. Offshore (farfield) rates were consistent with those measured in similar locations in the SCB (Ward, 1987) and coastal locations in Monterey Bay, California (Ward, 2005; Smith et al., 2014), but slightly lower than those measured within the California Current (Santoro et al., 2010). The rate of nitrification is light-inhibited and related to ammonium concentration (Ward, 2008). Our results are consistent with these traits, where nitrification rates show positive correlations with water column N species and negative correlations with DO and temperature (Spearman rank analysis; Figure S11). Random forest regressions explained a relatively low percentage of the variance for nitrification rates (20%; Figure S10). Phosphate and station type were most predictive, followed by temperature, nitrate + nitrite, and DO, likely related to nitrifying bacteria typically being light-inhibited and thus more abundant below the eutrophic zone, where water temperatures were colder and DO is lower (Ward, 1987, 2005; Santoro et al., 2010; Smith et al., 2014). The low percentage of the variability explained by the random forest models suggests that other factors affected the nitrification rates, such as the composition of the bacterial community (Ward, 2005) or possibly the added uncertainty of the underestimation of the rates due to insufficient spike as described above.

Wastewater N is predominantly ammonium and is discharged at depth, rising in a buoyant plume and generally trapped below the mixed layer (**Figure 3**; Nezlin et al., 2020). Because wastewater ammonium is discharged below the photic zone, wastewater ammonium was expected to be nitrified rapidly. Indeed, elevated nitrite concentrations and higher nitrification rates were associated with the OCSD effluent plume (McLaughlin et al., 2017), while effluent discharges in other coastal regions have led to similarly elevated nitrification rates in sediments near outfalls (Axelrad et al., 1981; Nowicki, 1994). Furthermore, an OCSD diversion study was able to track changes in nitrification rates when the plume was "turned-off" relative to "turned-on," with results suggesting that wastewater ammonium was nitrified on relatively short time scales of hours to days (McLaughlin et al., 2017). The contribution of nitrate from this nitrification of wastewater effluent has the potential to support significant productivity in coastal areas.

In this study, ammonium concentrations were elevated in nearfield stations relative to farfield stations, particularly at the depths associated with the plume (**Figure 3**). These high ammonium concentrations were associated with increased nitrification rates, both directly over the outfall and at a distance from the outfall but still within the plume, suggesting a local impact on N cycling from wastewater effluent discharges. Generally, the LACSD nitrification rates were higher than the OCSD rates, particularly below the thermocline, which is consistent with the higher concentrations of ammonium in effluent (Figure S9). However, OCSD had much greater variability in nitrification rates near its outfall compared to LACSD, with relatively high nitrification rates within the chlorophyll maximum and within the mixed layer, as well as the highest recorded nitrification rate in a bottom sample during spring 2015, demonstrating the variability present in the rates both within a site and across the region. Concentrations of nitrite, likely from oxidation of ammonium, were elevated within the plume over both outfalls and, as

noted above, did not show any seasonal variability, suggesting a continuous source (**Figure 3**). Nitrate concentrations were not significantly elevated in the nearfield relative to farfield stations; however, the concentrations of nitrate were 2–3 times higher than ammonium and 10 times higher than nitrite; thus, the additional contribution from nitrification if diluted over a larger area may not have been distinguishable from local heterogeneity in concentrations. Nitrification rates were not higher in the "fresh" plume compared to "older" plume stations, suggesting that the time scale of nitrification of plume ammonium was on the order of days and that the elevation in nitrification rates encompasses, at minimum, plume areas as defined by this study (i.e., detectable by CDOM).

The important role of regional factors in nitrate assimilation compared to localized impacts of wastewater plumes

Nitrate assimilation (incorporation of nitrate into the biomass) was not directly measured in this study; however, stable isotopes were employed as tracers of this process in the water column. The relationship between $\delta^{15}N_{NO2+NO3}$ and $\delta^{18}O_{NO2+NO3}$ was generally consistent with nitrate assimilation in the water column and was not significantly different between seasons and station location. The relative enrichments in $\delta^{15}N_{NO2+NO3}$ and $\delta^{18}O_{NO2+NO3}$ generally fell along a line with a slope of 1 (**Figures 5C** and S5), particularly during the spring 2016 sampling; however, the low surface values for $\delta^{15}N_{NO2+NO3}$ resulted in poor or negative correlations between $\delta^{15}N_{NO2+NO3}$ and $\delta^{18}O_{NO2+NO3}$ for some stations. A linear relationship between $\delta^{15}N_{NO2+NO3}$ and $\delta^{18}O_{NO2+NO3}$ with a slope of 1 would be predicted if phytoplankton assimilation or denitrification was the dominant process controlling the isotopic composition of nitrate (Granger et al., 2004). However, because concentrations of oxygen were relatively high (always greater than 2 mg L^{-1}), denitrification is not likely to be a significant process in these waters and the isotope affect is likely attributable to assimilation (Wankel et al., 2007). Because our oxygen isotope ratios for dissolved nitrate + nitrite were measured using the denitrifier method, the apparent $\delta^{18}O_{NO2+NO3}$ values reported may include some errors. Casciotti et al. (2007) noted that when nitrite was 2% or more of the total nitrate + nitrite present in the sample, the denitrifier method would give a detectable error in the apparent $\delta^{18}O_{NO2+NO3}$, underestimating the value. This source of error is a concern for 30% of our samples, particularly the nearfield stations (38%) where mean nitrite fraction of the nitrate + nitrite pool is 3.8%, though also the farfield stations (20%) where the mean nitrite fraction is 1.2%. The effect applies only to the oxygen isotope values and, assuming the offset would add 25% to the $\delta^{18}O$ of nitrite (as estimated by Cassioti et al., 2007), would increase $\delta^{18}O_{NO2+NO3}$ values by 0.08–13.8% with a mean increase of 2.69%, which would slightly reduce the spread of samples along the $\delta^{18}O_{NO2+NO3}$ axis of **Figure 5C** (Figure S13).

As indicated by patterns in $\delta^{15}N_{NO2+NO3}$ and $\delta^{18}O_{NO2+NO3}$, nitrate + nitrite assimilation was not significantly different in nearfield areas versus farfield areas but had clear seasonal patterns, suggesting that regional mixing and dilution of wastewater N likely spread the impact on assimilation over a much wider area, thereby creating a potential temporal lag in effect. During upwelling periods, particularly during spring 2016, the effect of assimilation on the isotopic composition of the dissolved nitrate pool is evident from the measurements of $\delta^{18}O_{NO2+NO3}$ falling along a 1:1 line (**Figures 5C** and S5). However, during the summer sampling periods, the isotope effect from assimilation of "new" nitrate from upwelling is diluted and the relationship between the two isotopes appears more influenced by nitrification (low $\delta^{15}N_{NO2+NO3}$ and high $\delta^{18}O_{NO2+NO3}$). In Monterey Bay, in northern California, nitrification of "natural" ammonium from regenerated organic matter was found to contribute approximately 30% of nitrate-based primary production (Wankel et al., 2007). The isotopic composition of dissolved nitrate at all stations increased with nitrate concentration and the fraction of nitrate in the DIN pool. This finding is consistent with nitrification as a significant driver defining the composition of the DIN pool and the isotopic composition thereof region-wide (Sugimoto et al., 2009; McLaughlin et al., 2017). However, because nitrification occurs largely below the euphotic zone, the importance of this source of nitrate for regional primary productivity will be directly related to physical mixing in the region. The time scale of when this subsurface nitrate source mixes into surface waters could result in impacts of this source in the farfield regions and not necessarily near the discharge location.

The regional scale impacts of anthropogenic nutrient inputs on the biogeochemical cycling of carbon and oxygen

Regional factors such as upwelling and Pacific Basin-scale changes in circulation have been shown to be the primary drivers for the concentrations of chlorophyll biomass and the depth of the chlorophyll maximum layer (Mantyla et al., 2008; Nezlin et al., 2012; Nezlin et al., 2018). This work highlights the importance of regional-scale influences on carbon and oxygen cycling. In this study, no statistically significant differences in instantaneous rates of primary productivity and respiration were found in nearfield versus farfield areas (**Figure 7**). This finding is consistent with an investigation of pH and aragonite saturation state during the same time period as this study, in which no significant differences were found between these parameters on the continental shelf (near anthropogenic discharges), compared to offshore of these influences (McLaughlin et al., 2018). While some regional differences were detected in chlorophyll *a* and DO, and mean chlorophyll fluorescence was elevated in proximity to the wastewater plume, variability among stations and seasons was high (**Figures 2** and S11). High variability is consistent with other research in the area, which has shown that physical mixing processes, such as internal waves, can create thin bands of high productivity along the coast and have

a significant effect on primary production over relatively small spatial scales (Lucas et al., 2011; Omand et al., 2011; Omand et al., 2012). The alteration of N:P ratios in nearfield regions could impact phytoplankton community productivity as noted above (Grosse et al., 2017; Moreno and Martiny, 2018; Fagan et al., 2019), resulting in a dilution of the impact of increased N over a larger area. Furthermore, we saw evidence of seasonal upwelling stimulating an increase in chlorophyll biomass and bringing intrusions of deep, cold waters that are low in DO into surface waters, impacting both nearfield and farfield regions. This evidence supports the hypothesis that regional mixing of water masses dilutes the impact of wastewater N on the coastal environment, which may also potentially be enhanced by outfall diffuser systems that discharge effluent over large areas, spreading the effect on primary production and respiration over larger areas and, by extension, carbon and oxygen cycling in the SCB (Mantyla et al., 2008; Nezlin et al., 2012; Nezlin et al., 2018).

Random forest regression characterized a low percentage of variance for both primary production and respiration (30% and 18%, respectively; Figure S12); thus, the observed parameters did not account for the primary drivers of variability in these processes or the relationships between factors are diluted regionally. Season was the most predictive variable of primary production in random forest analysis, indicating the importance of regional variables on primary productivity, as the SCB is subject to seasonal upwelling. This seasonality is shown in the spring and summer differences in temperature, salinity, and chlorophyll *a* concentration during the study (**Figure 2**). Station type was not very predictive for either primary production or respiration, suggesting that any impact of the wastewater plume is diluted across the region. This dilution effect is also apparent in the isotopic signature of the assimilation of "new" nitrate, as $\delta^{15}N_{NO2+NO3}$ is also mixed throughout the study area, particularly during summer periods of stratification (**Figure 5C**). Furthermore, concentrations of suspended particulate matter (carbon, nitrogen, and phosphorus) and nutrient ratios within that suspended matter were not significantly different in the nearfield versus the farfield (**Figures 4** and **5**). This decoupling of the presence of the wastewater plume and its associated nutrients from primary production, suspended organic matter, and respiration can be explained by regional dilution of effluent nitrogen due to water mass mixing. Both the LACSD and OCSD outfalls have multiport diffusers to disperse and increase dilution of the plume over a large area to minimize immediate local impacts of the discharge on the coastal ocean environment (Koh and Brooks, 1975). The relative buoyancy of the plume to local seawater traps the plume in the subsurface near the base of the euphotic zone where nutrients could be utilized by primary producers, but the impact is designed to be diluted over a larger area dictated by the local hydrodynamics of plume mixing as well as seasonal, basin-scale changes in currents and ocean state. Given that no difference was observed in primary production and respiration in plume-affected areas relative to farfield areas, the effect of effluent nutrients on these processes is likely diluted throughout the region into farfield areas or is too small to detect.

While most of the patterns in carbon and oxygen cycling were regional in scope, there was some evidence of local influence. Isotopic signatures of particulate matter ($\delta^{15}N_{PM}$ and $\delta^{13}C_{PM}$) were both slightly, but significantly, higher in the nearfield compared to farfield, potentially reflecting a small local influence on carbon and nitrogen cycling (**Figure 5**). Higher $\delta^{15}N_{PM}$ and $\delta^{13}C_{PM}$ values have been associated with higher primary productivity in coastal areas (Oczkowski et al., 2014; Oczkowski et al., 2016) and may be a more integrated metric of primary productivity differences than an instantaneous rate measurement. The isotopic composition of nitrogen in suspended material ($\delta^{15}N_{PM}$) is slightly lower than in dissolved nitrate + nitrite in the water column ($\delta^{15}N_{NO2+NO3}$), indicating the presence of a small isotopic discrimination associated with uptake of nitrate into the biomass (**Figure 5H**; Ostrom et al., 1997). The lighter isotope is preferentially utilized by phytoplankton: As N becomes limiting, this isotopic discrimination diminishes until the isotopic composition of the biomass is the same as that of the N being utilized (Ostrom et al., 1997), such that higher values are typically associated with more competition for N and higher primary production (Oczkowski et al., 2014; Oczkowski et al., 2016).

Both $\delta^{15}N_{PM}$ and $\delta^{13}C_{PM}$ increased with chlorophyll fluorescence (**Figure 5I** and **F**). Using chlorophyll *a* as a proxy for phytoplankton biomass, an increase in $\delta^{13}C_{PM}$ with biomass is consistent with lowering of dissolved inorganic carbon and dissolved carbon dioxide (Ostrom et al., 1997). Furthermore, chlorophyll *a* fluorescence was also slightly, but significantly, higher in the nearfield, which may reflect increased biomass in the nearshore. This effect has important implications for regional variability in acidification. Nutrient enrichment of coastal waters has been linked to impacts on the aragonite saturation state, inducing waters into undersaturated conditions when they otherwise might not have been (Cai et al., 2011; Wallace et al., 2014; Rheuban et al., 2019). Regionally, the SCB is exposed to waters with aragonite saturations states below thresholds thought to be important for marine calcifiers (McLaughlin et al., 2018), such that further investigation into potential enhancement of acidification associated with increased primary production is warranted.

The failings of a "reference-area" approach to document impacts of point sources on nutrient and carbon cycling

The study design was based on the hypothesis that areas near wastewater outfalls would be more impacted from nutrient discharges than areas spatially distant from the outfalls. Results suggest that such a concept has limitations. While nitrification, which occurs at depths directly associated with detectable plume, showed significant differences between nearfield and farfield stations, an immediate local effect on instantaneous rates of primary production and respiration was not observed. While a slight lag in the timing (and thus distance) of elevated primary production and chlorophyll *a* from wastewater N

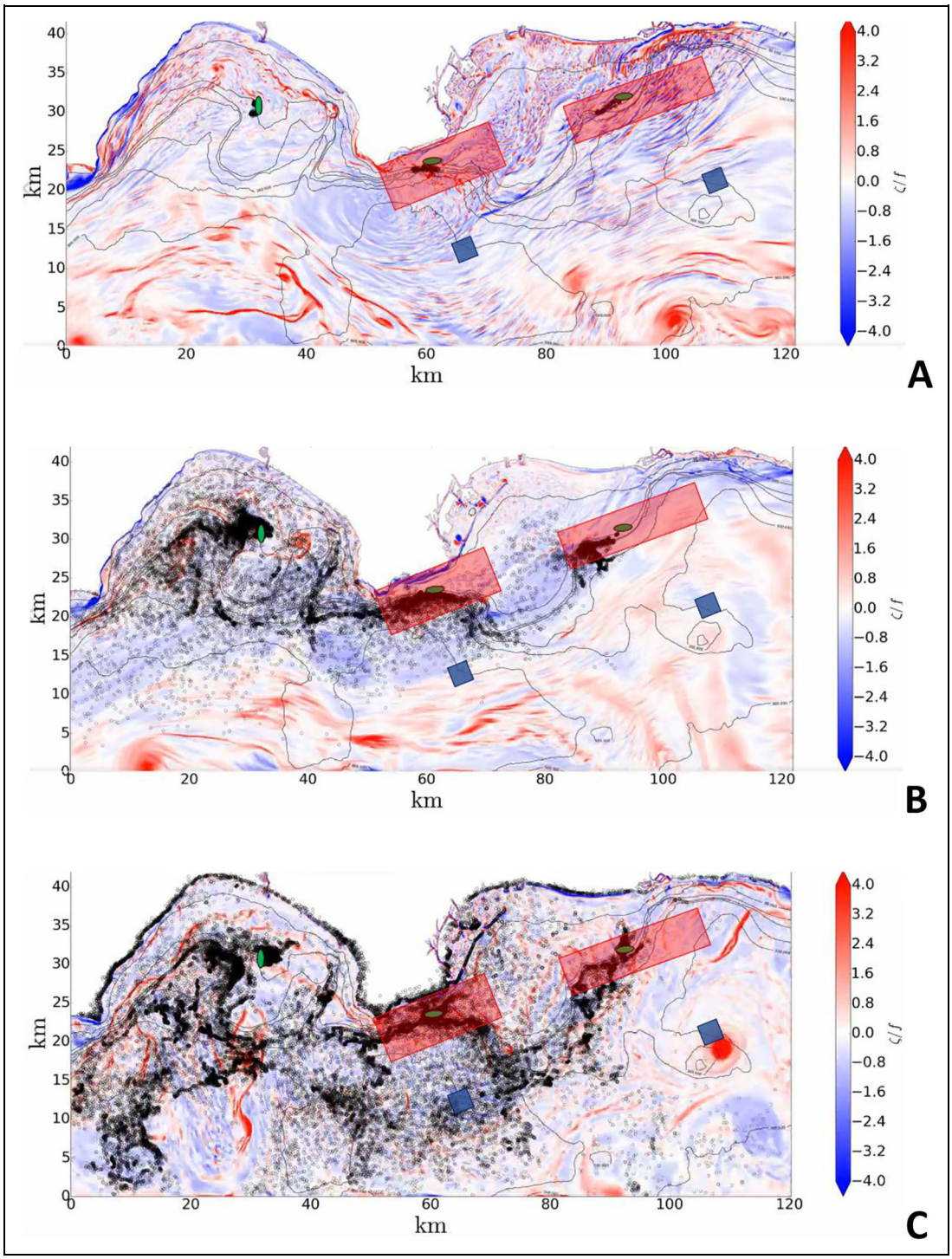

Figure 8. Downscaled regional ocean model demonstrating the fate of wastewater effluent released from ocean outfalls. The model (350-m scale), run in particle tracking mode, shows the distribution of particles (black circles) released from the outfalls (green ovals) at (A) 9 h from the start of the simulation on January 1 at 01:00); (B) 2 weeks into the simulation, when particles were nearly completely mixed in the nearshore areas; and (C) 2 months, the end of the simulation, when particles were mixed to the offshore regions (Dauhajre et al., 2019). Color bar represents the Coriolis-normalized vorticity, a measure of ocean stirring. Red boxes are nearfield areas and blue boxes represent farfield, offshore areas. DOI: https://doi.org/10.1525/elementa.2020.00145.f8

discharged by ocean outfalls at depth was expected, the observations suggest that levels of advection, stirring, and eventual mixing in the region were sufficient to transport anthropogenic nutrients to presumed "minimally disturbed" reference areas in the farfield. Thus, the concept of a "reference area" (Nezlin et al., 2020) as implemented here in the SCB is flawed for characterizing wastewater nutrient impacts on these processes. This conclusion is supported by numerical ocean model simulations from the Regional Ocean Modeling System (www.myroms.org;

Shchepetkin and McWilliams, 2005) run in particle tracking mode to track Lagrangian flow of "plume particles" (**Figure 8**). When particles were released from the outfalls, they were transported to farfield areas used for this study on timescales of weeks to months, suggesting that wastewater N is mixed over larger regional scales. In such cases, impacts of anthropogenic nutrients on primary production, related elevation in respiration, and impacts on carbon cycling and acidification, are not easily deciphered with observational data alone. Thus, the monitoring scheme to assess nutrient impacts should be reevaluated to include modeling approaches that can account for the complexity of mixing and farfield transport in the region.

Conclusion

In this study, we found that wastewater nutrient inputs have an immediate, local effect on nutrient stoichiometry and nitrogen concentrations and elevated rates of nitrification within the plume. Impact of wastewater plumes on nitrate assimilation, primary production, chlorophyll *a*, respiration, and DO was moderated, however, by regional mixing of water masses. This finding lends strong support for further study of local anthropogenic forcing through ocean numerical modeling studies, given the difficulty of disentangling local to global scale drivers through observations alone (Chan et al., 2016). While observational studies such as this one are costly, they provide key data needed to evaluate the accuracy and utility of ocean numerical models. These data should not only include state variables, which can be used to characterize the uncertainty in model output, but also rate variables, which can be used to determine whether the model configuration accurately represents the underlying biogeochemical processes creating that output.

Data accessibility statement

This study was done in collaboration with the Southern California Bight Regional Marine Monitoring Program, a collaborative monitoring program whose goal is to collect regional-scale data on the health of coastal habitats that can be used to make better management decisions. Pursuant to this goal, all data are publicly available on the Southern California Coastal Water Research Project website: www.sccwrp.org.

Supplemental files

The supplemental files for this article can be found as follows:

Figure S1. Spatial extent of the effluent plumes during each sampling event as measured by colored dissolved organic matter (mg m^{-3}). Note colored scale on each graphic is different, as scaling was free on each figure to demonstrate the extent of the plume. Scales are plotted from the minimum reported value to the maximum for each site to identify the plume locations over each outfall. Each conductivity-temperature-depth cast location is represented by a black vertical line; multiple casts were taken to determine the direction of the plume during sampling events and not all stations correspond to sampling locations on **Figure 1**. The station sampled over each outfall is highlighted in red.

Figure S2. Timing of sampling and ranges of data for upper 60 m at each site. Black dot represents the mean and black bar, the standard deviation of all values in the upper 60 m.

Figure S3. Depth profiles of particulate carbon, nitrogen, and phosphorus. Plume is generally located between depths of 20 and 60 m in the nearfield sites.

Figure S4. Depth profiles of particulate C:N, C:P, and N:P. Plume is generally located between depths of 20 and 60 m in the nearfield sites.

Figure S5. The $\delta^{15}N_{NO2+NO3}$ as a function of nitrate concentration, N^*, nitrification rate, and $\delta^{18}O_{NO2+NO3}$. The black line in the far-right panels represents the 1:1 relationship between the relative enrichment of the two isotopes. The size of the points represents the fraction of nitrite in the nitrite + nitrate measured in each sample; larger points have higher fraction of nitrite.

Figure S6. Depth profiles of the stable isotopic composition of particulate carbon ($\delta^{13}C_{PM}$) and nitrogen ($\delta^{15}N_{PM}$). Plume is generally located at depths between 20 and 60 m in the nearfield sites.

Figure S7. $\delta^{15}N_{PM}$ as a function of particulate nitrogen concentration, dissolved inorganic nitrogen, $\delta^{15}N_{NO2+NO3}$, and chlorophyll *a* concentration.

Figure S8. $\delta^{13}C_{PM}$ as a function of particulate carbon, dissolved inorganic nitrogen, $\delta^{15}N_{PM}$, and chlorophyll *a* concentration.

Figure S9. Depth-integrated primary production rates (A), average subsurface respiration rates (B), and nitrification rates faceted by depth layer (C) by season and by station. No rates of primary production were measured in summer 2014. Error bars indicate the standard deviation of triplicate samples.

Figure S10. Relationship between depth-integrated primary production and average subsurface respiration. Measurements of both parameters were available only for the three time periods indicated.

Figure S11. Spearman rank correlations between dissolved and particulate variables. Color scale indicates the correlation coefficient, where red indicates a positive correlation, blue indicates a negative one, and white is 0 for no correlation. Asterisks indicate significance where $^*P < 0.05$, $^{**}P < 0.01$, and $^{***}P < 0.001$. Parameters are ordered using hierarchical clustering.

Figure S12. Variable importance from random forest regression models predicting primary production (A), respiration (B), and nitrification (C). Predictor variables were plotted with their increase in percent mean squared error (%IncMSE) when the variable was randomly permuted in the model; higher values indicate the variables that were more important to the regression. The overall percent variance explained using the random forest models was 30% for primary production, 18% for respiration, and 20% for nitrification.

Figure S13. Estimation of the impact of high nitrite on the $\delta^{18}O_{NO2+NO3}$. For samples with high nitrite concentrations, the denitrification method employed in this study for oxygen isotope analysis of dissolved nitrate + nitrite is

expected to underestimate the oxygen isotopic composition of nitrite by 25–30%. We calculated the fraction of nitrite in each sample and estimated the impact of a 25% underestimation of the $\delta^{18}O_{NO2}$ on the final $\delta^{18}O_{NO2+NO3}$ (Adj $\delta^{18}O_{NO2+NO3}$, right panels). Values were increased an average of 2.7% with a maximum increase of 13.8%. Samples with the highest fraction of nitrite (indicated by the size of the point) had the greatest increase.

Acknowledgments

The authors thank field sampling and laboratory personnel from the following organizations: City of San Diego, Orange County Sanitation District, Los Angeles County Sanitation Districts, and the Southern California Coastal Water Research Project. We also want to thank members of the Southern California Bight 2013 Regional Marine Monitoring Program Nutrients and Water Quality Committee who contributed thoughtful comments on study design, data analysis and interpretation, and early drafts of this article. We also thank two anonymous reviewers and Dr Jody Deming for their comments to improve this article.

Funding

Funding for this project was provided from Orange County Sanitation District, Los Angeles County Sanitation Districts, and the Southern California Coastal Water Research Project.

Competing interests

Dr Martha Sutula is an editor in the Ecology and Earth Systems domain, and the lead author's husband, Dr Steven Allison, is editor-in-chief for that same domain.

Author contributions

Karen McLaughlin was the co-lead on this project with Meredith D. A. Howard. Karen McLaughlin contributed to study design, led the study of nutrient and stable isotope analyses and nitrification rates, conducted the data analysis and drafted the article.

Meredith D.A. Howard was the co-lead on the project with Karen McLaughlin. She contributed to study design, managed project budget, coordinated the field work and led the primary production and respiration portions of the study. She contributed to primary production and respiration sections of the article and reviewed the final draft.

George Robertson coordinated field sampling with the Sanitation Districts, contributed to study design, reviewed data analysis plan and preliminary data, and reviewed the article on behalf of management agencies.

Carly D. A. Beck was the lead research technician on the project. She contributed to study design, managed field staff in the field, and coordinated data collection and quality assurance and reviewed the final article.

Minna Ho is a partner on the modeling effort. She provided the particle tracking model output and interpretation of the observational data.

Fayçal Kessouri is the lead modeler working on nutrient impacts on coastal environments. He engineered the regional oceanic modeling system used for particle tracking model output and interpretation of the observational data.

Nikolay P. Nezlin contributed data analysis for the nitrification study and analysis of water column profiles.

Martha Sutula is the Principal Investigator of the Biogeochemistry Department at Southern California Coastal Water Research Project, Costa Mesa. She contributed project management, study design, and drafted portions of the final report.

Stephen B. Weisberg is the Executive Director at SCCWRP, he contributed project management, coordination with stakeholders, and reviewed the final draft.

All authors contributed critically to the manuscript and approved its submission.

References

Anderson, CR, Brzezinski, MA, Washburn, L, Kudela, R. 2006. Circulation and environmental conditions during a toxigenic *Pseudo-nitzschia australis* bloom in the Santa Barbara Channel, California. *Marine Ecology Progress Series* **327**: 119–133.

Axelrad, D, Poore, G, Arnott, G, Bauld, J, Brown, V, Edwards, R, Hickman, N. 1981. The effects of treated sewage discharge on the biota of Port Phillip Bay, Victoria, Australia, in Neilson, BJ, Cronin, LE eds., *Estuaries and nutrients*. Totowa, New Jersey: Humana Press: 279–306.

Boesch, DF. 2019. Barriers and bridges in abating coastal eutrophication. *Frontiers in Marine Science* **6**: 123.

Bograd, SJ, Castro, CG, Di Lorenzo, E, Palacios, DM, Bailey, H, Gilly, W, Chavez, FP. 2008. Oxygen declines and the shoaling of the hypoxic boundary in the California Current. *Geophysical Research Letters* **35**: L12607.

Booth, JAT, Woodson, CB, Sutula, M, Micheli, F, Weisberg, SB, Bograd, SJ, Steele, A, Schoen, J, Crowder, LB. 2014. Patterns and potential drivers of declining oxygen content along the southern California coast. *Limnology and Oceanography* **59**: 1127–1138.

Borges, AV, Gypens, N. 2010. Carbonate chemistry in the coastal zone responds more strongly to eutrophication than to ocean acidification. *Limnology and Oceanography* **55**: 346–353.

Breiman, L. 2001. Random forests. *Machine Learning* **45**: 5–32.

Breitburg, D, Levin, LA, Oschlies, A, Grégoire, M, Chavez, FP, Conley, DJ, Garçon, V, Gilbert, D, Gutiérrez, D, Isensee, K. 2018. Declining oxygen in the global ocean and coastal waters. *Science* **359**(6371): eaam7240. DOI: http://dx.doi.org/10.1126/science/aam7240.

Brzezinski, MA, Washburn, L. 2011. Phytoplankton primary productivity in the Santa Barbara channel: Effects of wind-driven upwelling and mesoscale eddies. *Journal of Geophysical Research: Oceans* **116**: C12.

Cai, WJ, Hu, XP, Huang, WJ, Murrell, MC, Lehrter, JC, Lohrenz, SE, Chou, WC, Zhai, WD, Hollibaugh, JT, Wang, YC, Zhao, PS, Guo, XH, Gundersen, K,

Dai, MH, Gong, GC. 2011. Acidification of subsurface coastal waters enhanced by eutrophication. *Nature Geoscience* **4**: 766–770.

Capone, DG, Hutchins, DA. 2013. Microbial biogeochemistry of coastal upwelling regimes in a changing ocean. *Nature Geoscience* **6**: 711–717.

Casciotti, KL, Böhlke, JK, McIlvin, MR, Mroczkowski, SJ, Hannon, JE. 2007. Oxygen isotopes in nitrite: Analysis, calibration, and equilibration. *Analytical Chemistry* **79**(6): 2427–2436.

Casciotti, KL, Sigman, DM, Hastings, MG, Bohlke, JK, Hilkert, A. 2002. Measurement of the oxygen isotopic composition of nitrate in seawater and freshwater using the denitrifier method. *Analytical Chemistry* **74**: 4905–4912.

Chan, F, Boehm, AB, Barth, JA, Chornesky, EA, Dickson, AG, Feely, RA, Hales, B, Hill, TM, Hofmann, G, Ianson, D, Klinger, T, Largier, J, Newton, J, Pedersen, TF, Somero, GN, Sutula, M, Wakefield, WW, Waldbusser, GG, Weisberg, SB, Whiteman, EA. 2016. *The West Coast ocean acidification and hypoxia science panel: Major findings, recommendations, and actions*. Oakland, CA: West Coast Environmental Law Research Foundation.

Chavez, FP, Messié, M. 2009. A comparison of eastern boundary upwelling ecosystems. *Progress in Oceanography* **83**: 80–96.

Coplen, TB, Qi, H, Révész, K, Casciotti, K, Hannon, JE. 2012. Determination of the $\delta^{15}N$ and $\delta^{18}O$ of nitrate in water; RSIL lab code 2900, in Révész, K, Coplen, TB eds., *Methods of the Reston Stable Isotope Laboratory: U.S. Geological Survey Techniques and Methods Book No. 10 Stable Isotope-Ratio Methods Section C, Chapter 17.* Reston, VA: U.S. Geological Survey: 35 (Supersedes version 1.0 released in 2007).

Cullen, J, Eppley, R. 1981. Chlorophyll maximum layers of the Southern-California Bight and possible mechanisms of their formation and maintenance. *Oceanologica Acta* **4**: 23–32.

Cutler, DR, Edwards, TC, Beard, KH, Cutler, A, Hess, KT, Gibson, J, Lawler, JJ. 2007. Random forests for classification in ecology. *Ecology* **88**: 2783–2792.

Dauhajre, DP, McWilliams, JC, Renault, L. 2019. Nearshore Lagrangian connectivity: Submesoscale influence and resolution sensitivity. *Journal of Geophysical Research: Oceans* **124**: 5180–5204.

Deutsch, C, Frenzel, H, McWilliams, JC, Renault, L, Kessouri, F, Howard, E, Liang, J-H, Bianchi, D, Yang, S. 2021. Biogeochemical variability in the California Current system. *Progress in Oceanography*: 102565. DOI: http://dx.doi.org/10.1101/2020.02.10.942565.

Deutsch, C, Gruber, N, Key, RM, Sarmiento, JL, Ganachaud, A. 2001. Denitrification and N_2 fixation in the Pacific Ocean. *Global Biogeochemical Cycles* **15**: 483–506.

Diaz, RJ, Rosenberg, R. 2008. Spreading dead zones and consequences for marine ecosystems. *Science* **321**(5891): 926–929.

Eppley, RW. 1992. Chlorophyll, photosynthesis and new production in the Southern California Bight. *Progress in Oceanography* **30**: 117–150.

Fagan, AJ, Moreno, AR, Martiny, AC. 2019. Role of ENSO conditions on particulate organic matter concentrations and elemental ratios in the Southern California Bight. *Frontiers in Marine Science* **6**: 386.

Fehling, J, Davidson, K, Bolch, CJ, Bates, SS. 2004. Growth and domoic acid production by *Pseudonitzschia seriata* (Bacillariophyceae) under phosphate and silicate limitation. *Journal of Phycology* **40**: 674–683.

Fennel, K, Testa, JM. 2019. Biogeochemical controls on coastal hypoxia. *Annual Review of Marine Science* **11**: 105–130.

Glibert, PM, Harrison, J, Heil, C, Seitzinger, S. 2006. Escalating worldwide use of urea—A global change contributing to coastal eutrophication. *Biogeochemistry* **77**: 441–463.

Goldman, JC, Caron, DA, Dennett, MR. 1987. Regulation of gross growth efficiency and ammonium regeneration in bacteria by substrate C:N ratio. *Limnology and Oceanography* **32**: 1239–1252.

Granger, J, Sigman, DM, Needoba, JA, Harrison, PJ. 2004. Coupled nitrogen and oxygen isotope fractionation of nitrate during assimilation by cultures of marine phytoplankton. *Limnology and Oceanography* **49**: 1763–1773.

Grosse, J, Burson, A, Stomp, M, Huisman, J, Boschker, HT. 2017. From ecological stoichiometry to biochemical composition: Variation in N and P supply alters key biosynthetic rates in marine phytoplankton. *Frontiers in Microbiology* **8**: 1299.

Gruber, N, Sarmiento, JL. 1997. Global patterns of marine nitrogen fixation and denitrification. *Global Biogeochemical Cycles* **11**: 235–266.

Hannon, JE, Böhlke, JK. 2008. Determination of the delta (15N/14N) of ammonium (NH4+) in water: RSIL Lab Code 2898, in Révész, K, Coplen, TB eds., *Methods of the Reston Stable Isotope Laboratory: U.S. Geological Survey Techniques and Methods Book No. 10 Stable Isotope-Ratio Methods Section C, Chapter 15*. Reston, VA: U.S. Geological Survey: 30.

Harrell, FE. 2014. Hmisc: A package of miscellaneous R functions. R Package Version 4.5-0. CRAN.

Henriksen, K, Kemp, WM. 1988. Nitrification in estuarine and coastal marine sediments, in Blackburn, TH, Sorensen, J eds., *Nitrogen cycling in coastal marine environments*. New York, NY: John Wiley: 207–249.

Holmes, RM, Aminot, A, Kerouel, R, Hooker, BA, Peterson, BJ. 1999. A simple and precise method for measuring ammonium in marine and freshwater ecosystems. *Canadian Journal of Fisheries and Aquatic Sciences* **56**: 1801–1808.

Howard, MDA, Sutula, M, Caron, DA, Chao, Y, Farrara, JD, Frenzel, H, Jones, B, Robertson, G, McLaughlin, K, Sengupta, A. 2014. Anthropogenic nutrient sources rival natural sources on small scales in the coastal waters of the Southern California Bight. *Limnology and Oceanography* **59**: 285–297.

Howarth, RW, Sharpley, A, Walker, D. 2002. Sources of nutrient pollution to coastal waters in the United States: Implications for achieving coastal water quality goals. *Estuaries* **25**: 656–676.

Kelley, D, Richards, C. 2017. Oce: Analysis of oceanographic data. R package version 0.9–21. Available at https://CRAN.R-project.org/package=oce.

Kelly, RP, Foley, M, Fisher, W, Feely, R, Halpern, B, Waldbusser, G, Caldwell, M. 2011. Mitigating local causes of ocean acidification with existing laws. *Science* **332**: 1036–1037.

Kessouri, F, McLaughlin, K, Sutula, MA, Bianchi, D, Ho, M, McWilliams, JC, Renault, L, Molemaker, J, Deutsch, CA, Leinweber, A. 2020. Configuration and validation of an oceanic physical and biogeochemical model to investigate coastal eutrophication: Case study in the Southern California Bight. *Earth and Space Science Open Archive*. DOI: http://dx.doi.org/10.1002/essoar.10504012.1.

Koch, SE, desJardins, M, Kocin, PJ. 1983. An interactive Barnes objective map analysis scheme for use with satellite and conventional data. *Journal of Applied Meteorology and Climatology* **22**: 1487–1503.

Koh, RC, Brooks, NH. 1975. Fluid mechanics of wastewater disposal in the ocean. *Annual Review of Fluid Mechanics* **7**: 187–211.

Liaw, A, Wiener, M. 2012. Random forest: Breiman and Cutler's random forests for classification and regression. R Package Version 4.6-7. CRAN.

Los Angeles County Sanitation Districts. 2014. *2014 Pretreatment program annual report*. Whittier, CA. Available at https://www.lacsd.org/services/wastewater/wwpubreports/iwannualrpts.asp.

Los Angeles County Sanitation Districts. 2015. *2015 Pretreatment program annual report*. Whittier, CA. Available at https://www.lacsd.org/services/wastewater/wwpubreports/iwannualrpts.asp.

Los Angeles County Sanitation Districts. 2016. *2016 Pretreatment program annual report*. Whittier, CA. Available at: https://www.lacsd.org/services/wastewater/wwpubreports/iwannualrpts.asp.

Lucas, AJ, Franks, PJ, Dupont, CL. 2011. Horizontal internal-tide fluxes support elevated phytoplankton productivity over the inner continental shelf. *Limnology and Oceanography: Fluids and Environments* **1**(1): 56–74.

Mantyla, AW, Bograd, SJ, Venrick, EL. 2008. Patterns and controls of chlorophyll-a and primary productivity cycles in the Southern California Bight. *Journal of Marine Systems* **73**: 48–60.

McLaughlin, K, Nezlin, NP, Howard, MD, Beck, CD, Kudela, RM, Mengel, MJ, Robertson, GL. 2017. Rapid nitrification of wastewater ammonium near coastal ocean outfalls, Southern California, USA. *Estuarine, Coastal and Shelf Science* **186**: 263–275.

McLaughlin, K, Nezlin, NP, Weisberg, SB, Dickson, AG, Booth, JAT, Cash, CL, Feit, A, Gully, JR, Howard, MD, Johnson, S. 2018. Seasonal patterns in aragonite saturation state on the Southern California continental shelf. *Continental Shelf Research* **167**: 77–86.

Moreno, AR, Martiny, AC. 2018. Ecological stoichiometry of ocean plankton. *Annual Review of Marine Science* **10**: 43–69.

Nezlin, N, Sutula, MA, Stumpf, RP, Sengupta, A. 2012. Phytoplankton blooms detected by SeaWiFS along the central and southern California coast. *Journal of Geophysical Research* **117**: C07004.

Nezlin, NP, Beegan, C, Feit, A, Gully, JR, Latker, A, McLaughlin, K, Mengel, MJ, Robertson, GL, Steele, A, Weisberg, SB. 2020. Colored dissolved organic matter (CDOM) as a tracer of effluent plumes in the coastal ocean. *Regional Studies in Marine Science* **35**: 101163.

Nezlin, NP, McLaughlin, K, Booth, JAT, Cash, CL, Diehl, DW, Davis, KA, Feit, A, Goericke, R, Gully, JR, Howard, MD. 2018. Spatial and temporal patterns of chlorophyll concentration in the Southern California Bight. *Journal of Geophysical Research: Oceans* **123**: 231–245.

Nowicki, BL. 1994. The effect of temperature, oxygen, salinity, and nutrient enrichment on estuarine denitrification rates measured with a modified nitrogen gas flux technique. *Estuarine, Coastal and Shelf Science* **38**: 137–156.

Oczkowski, A, Kreakie, B, McKinney, RA, Prezioso, J. 2016. Patterns in stable isotope values of nitrogen and carbon in particulate matter from the Northwest Atlantic continental shelf, from the Gulf of Maine to Cape Hatteras. *Frontiers in Marine Science* **3**: 252.

Oczkowski, A, Markham, E, Hanson, A, Wigand, C. 2014. Carbon stable isotopes as indicators of coastal eutrophication. *Ecological Applications* **24**(3): 457–466.

Omand, MM, Feddersen, F, Guza, RT, Franks, PJS. 2012. Episodic vertical nutrient fluxes and nearshore phytoplankton blooms in Southern California. *Limnology and Oceanography* **57**(6): 1673–1688.

Omand, MM, Leichter, JJ, Franks, PJ, Guza, RT, Lucas, AJ, Feddersen, F. 2011. Physical and biological processes underlying the sudden surface appearance of a red tide in the nearshore. *Limnology and Oceanography* **56**(3): 787–801.

Orange County Santitation District. 2015. 2014–2015 Annual report. Fountain Valley, CA: Environmental Compliance Division. Pretreatement program. Available at https://www.ocsan.gov/education/reports-agency-information/-folder-396.

Orange County Santitation District. 2016. 2015–2016 Annual report. Fountain Valley, CA: Environmental Compliance Division. Pretreatement program. Available at https://www.ocsan.gov/education/reports-agency-information/-folder-396.

Ostrom, NE, Macko, SA, Deibel, D, Thompson, RJ. 1997. Seasonal variation in the stable carbon and nitrogen isotope biogeochemistry of a coastal cold ocean environment. *Geochimica et Cosmochimica Acta* **61**: 2929–2942.

Patton, C, Kryskalla, JR. 2003. *Methods of analysis by the U.S. Geological Survey National Water Quality Laboratory: Evaluation of alkaline persulfate digestion as an alternative to Kjeldahl digestion for determination of total and dissolved nitrogen and phosphorus in water* (vol. 3, no. 4174). Denver, CO: U.S. Department of the Interior, U.S. Geological Survey.

Powley, HR, Dürr, HH, Lima, AT, Krom, MD, Van Cappellen, P. 2016. Direct discharges of domestic wastewater are a major source of phosphorus and nitrogen to the Mediterranean Sea. *Environmental Science & Technology* **50**: 8722–8730.

Prasad, AM, Iverson, LR, Liaw, A. 2006. Newer classification and regression tree techniques: Bagging and random forests for ecological prediction. *Ecosystems* **9**: 181–199.

Provoost, P, Van Heuven, S, Soetaert, K, Laane, R, Middelburg, J. 2010. Seasonal and long-term changes in pH in the Dutch coastal zone. *Biogeosciences* **7**: 3869.

R Core Team. 2019. *R: A language and environment for statistical computing*. R Foundation for Statistical Computing. Vienna, Austria. Available at https://www.R-project.org/.

Rabalais, NN, Cai, W-J, Carstensen, J, Conley, DJ, Fry, B, Hu, X, Quinones-Rivera, Z, Rosenberg, R, Slomp, CP, Turner, RE. 2014. Eutrophication-driven deoxygenation in the coastal ocean. *Oceanography* **27**: 172–183.

Redfield, AC. 1958. The biological control of chemical factors in the environment. *American Scientist* **46**: 205–221.

Rheuban, JE, Doney, SC, McCorkle, DC, Jakuba, RW. 2019. Quantifying the effects of nutrient enrichment and freshwater mixing on coastal ocean acidification. *Journal of Geophysical Research: Oceans* **124**(12): 9085–9100.

Roberts, PJ, Salas, HJ, Reiff, FM, Libhaber, M, Labbe, A, Thomson, JC. 2010. *Marine wastewater outfalls and treatment systems*. London, UK: International Water Association .

Robinson, C. 2019. Microbial respiration, the engine of ocean deoxygenation. *Frontiers in Marine Science* **5**: 533.

Rogowski, P, Terrill, E, Otero, MP, Hazard, L, Middleton, W. 2012. Mapping ocean outfall plumes and their mixing using autonomous underwater vehicles. *Journal of Geophysical Research Oceans* **117**: 1–12.

Rogowski, P, Terrill, E, Otero, MP, Hazard, L, Middleton, W. 2013. Ocean outfall plume characterization using an autonomous underwater vehicle. *Water Science and Technology* **67**: 925–933.

Santoro, AE, Casciotti, KL, Francis, CA. 2010. Activity, abundance and diversity of nitrifying archaea and bacteria in the central California Current. *Environmental Microbiology* **12**: 1989–2006.

Schnetzer, A, Jones, BH, Schaffner, RA, Cetinic, I, Fitzpatrick, E, Miller, PE, Seubert, EL, Caron, DA. 2013. Coastal upwelling linked to toxic *Pseudonitzschia australis* blooms in Los Angeles coastal waters, 2005–2007. *Journal of Plankton Research* **35**: 1080–1092.

Schnetzer, A, Miller, PE, Schaffner, RA, Stauffer, BA, Jones, BH, Weisberg, SB, DiGiacomo, PM, Berelson, WM, Caron, DA. 2007. Blooms of *Pseudonitzschia* and domoic acid in the San Pedro Channel and Los Angeles harbor areas of the Southern California Bight, 2003–2004. *Harmful Algae* **6**: 372–387.

Shchepetkin, AF, McWilliams, JC. 2005. The regional oceanic modeling system (ROMS): A split-explicit, free-surface, topography-following-coordinate oceanic model. *Ocean modelling* **9**: 347–404.

Sigman, DM, Granger, J, DiFiore, PJ, Lehmann, MM, Ho, R, Cane, G, van Geen, A. 2005. Coupled nitrogen and oxygen isotope measurements of nitrate along the eastern North Pacific margin. *Global Biogeochemical Cycles* **19**(4): GB4022.

Smith, J, Connell, P, Evans, RH, Gellene, AG, Howard, MDA, Jones, BH, Kaveggia, S, Palmer, L, Schnetzer, A, Seegers, BN, Seubert, EL, Tatters, AO, Caron, DA. 2018. A decade and a half of *Pseudonitzschia* spp. and domoic acid along the coast of southern California. *Harmful Algae* **79**: 87–104.

Smith, JM, Casciotti, KL, Chavez, FP, Francis, CA. 2014. Differential contributions of archaeal ammonia oxidizer ecotypes to nitrification in coastal surface waters. *The ISME Journal* **8**: 1704.

Smith, R, Eppley, R, Baker, K. 1982. Correlation of primary production as measured aboard ship in southern California coastal waters and as estimated from satellite chlorophyll images. *Marine Biology* **66**: 281–288.

Strong, AL, Kroeker, KJ, Teneva, LT, Mease, LA, Kelly, RP. 2014. Ocean acidification 2.0: Managing our changing coastal ocean chemistry. *Bioscience* **64**: 581–592.

Sugimoto, R, Kasai, A, Miyajima, T, Fujita, K. 2009. Controlling factors of seasonal variation in the nitrogen isotope ratio of nitrate in a eutrophic coastal environment. *Estuarine Coastal and Shelf Science* **85**: 231–240.

Sunda, WG, Cai, W-J. 2012. Eutrophication induced CO_2-acidification of subsurface coastal waters: Interactive effects of temperature, salinity, and atmospheric pCO_2. *Environmental Science & Technology* **46**: 10651–10659.

Sutton, A, Wanninkhof, R, Sabine, C, Feely, R, Cronin, M, Weller, R. 2017. Variability and trends in surface seawater pCO_2 and CO_2 flux in the Pacific Ocean. *Geophysical Research Letters* **44**: 5627–5636.

Sutula, M, Ho, M, Sengupta, A, Kessouri, F, McLaughlin, K, McCune, K, Bianchi, D. 2021. Dataset of terrestrial fluxes of freshwater, nutrients, carbon, and iron to the Southern California bight, USA. *Data in Brief* **35**: 106802.

Thomas, WH, Seibert, DL, Dodson, AN. 1974. Phytoplankton enrichment experiments and bioassays in

natural coastal sea water and in sewage outfall receiving waters off Southern California. *Estuarine and Coastal Marine Science* **2**: 191–206.

Valiela, I, Owens, C, Elmstrom, E, Lloret, J. 2016. Eutrophication of Cape Cod estuaries: Effect of decadal changes in global-driven atmospheric and local-scale wastewater nutrient loads. *Marine Pollution Bulletin* **110**: 309–315.

Waldbusser, GG. 2011. The causes of acidification in Chesapeake Bay and consequences to oyster shell growth and dissolution. *Journal of Shellfish Research* **30**: 559–560.

Waldbusser, GG, Bergschneider, H, Green, MA. 2010. Size-dependent pH effect on calcification in post-larval hard clam *Mercenaria* spp. *Marine Ecology Progress Series* **417**: 171–182.

Wallace, RB, Baumann, H, Grear, JS, Aller, RC, Gobler, CJ. 2014. Coastal ocean acidification: The other eutrophication problem. *Estuarine, Coastal and Shelf Science* **148**: 1–13.

Wankel, SD, Kendall, C, Francis, CA, Paytan, A. 2006. Nitrogen sources and cycling in the San Francisco Bay estuary: A nitrate dual isotopic composition approach. *Limnology and Oceanography* **51**: 1654–1664.

Wankel, SD, Kendall, C, Pennington, JT, Chavez, FP, Paytan, A. 2007. Nitrification in the euphotic zone as evidenced by nitrate dual isotopic composition: Observations from Monterey Bay, California. *Global Biogeochemical Cycles* **21**(2): GB2009.

Ward, BB. 1987. Nitrogen transformations in the Southern California Bight. *Deep-Sea Research* **34**: 785–805.

Ward, BB. 2005. Temporal variability in nitrification rates and related biogeochemical factors in Monterey Bay, California, USA. *Marine Ecology Progress Series* **292**: 97–109.

Ward, BB. 2008. Chapter 5, Nitrification in marine systems, in Capone, DG, Bronk, DA, Mulholland, MR, Carpenter, EJ eds., *Nitrogen in the marine environment*. Second edition. Burlington, MA: Elsevier: 199–261.

Wickham, H, Averick, M, Bryan, J, Chang, W, McGowan, LD, François, R, Grolemund, G, Hayes, A, Henry, L, Hester, J, Kuhn, M, Pedersen, TL, Miller, E, Bache, SM, Müller, K, Ooms, J, Robinson, D, Seidel, DP, Spinu, V, Takahashi, K, Vaughan, D, Wilke, C, Woo, K, Yutani, H. 2019. Welcome to the tidyverse. *Journal of Open Source Software* **4**(43): 1686. DOI: http://dx.doi.org/10.21105/joss.01686.

Wood, IR, Bell, RG, Wilkinson, DL. 1993. *Ocean disposal of wastewater*. Singapore: World Scientific.

United Nations World Water Assessment Programme. 2017. *The United Nations world water development report 2017: Wastewater, the untapped resource*. Paris, France: United Nations Educational, Scientific and Cultural Organization.

How to cite this article: McLaughlin, K, Howard, MDA, Robertson, G, Beck, CDA, Ho, M, Kessouri, F, Nezlin, NP, Sutula, M, Weisberg, SB. 2021. Influence of anthropogenic nutrient inputs on rates of coastal ocean nitrogen and carbon cycling in the Southern California Bight, United States. *Elementa: Science of Anthropocene* 9(1). DOI: https://doi.org/10.1525/elementa.2020.00145

Domain Editor-in-Chief: Jody W. Deming, University of Washington, Seattle, WA, USA

Associate Editor: Julie E. Keister, Biological Oceanography, University of Washington, Seattle, WA, USA

Knowledge Domain: Ocean Science

Published: July 30, 2021 **Accepted:** June 11, 2021 **Submitted:** September 25, 2020

ELEMENTA Science of the Anthropocene

Elem Sci Anth is a peer-reviewed open access journal published by University of California Press.

OPEN ACCESS